Project MC1.02121

Springback: Improvement of its Predictability to Meet
Industrial Requirements

Numerical Trimming Operation with Respect to Springback

Author   Marianna Avetisyan
              Netherlands Institute for Metals Research

Date   2004

Contents

Introduction

In the automotive industry, guidelines and finite element software are used in the design process of new sheet metal parts. Currently, the accuracy and reliability of these guidelines and numerical calculations do not satisfy the industrial requirements. The cornerstone of this problem lays in the deficient description of such phenomena as tearing, wrinkling, springback and other surface and geometric defects in numerical simulations of sheet metal forming processes.

1.1   Springback

Springback is a growing concern as manufacturers increasingly introduce materials with higher strength-to-modulus ratios in order to meet goals of improved fuel economy, emission, and safety. In this respect, high-strength low alloy steel (HSLA) and various aluminum alloys are frequently considered as direct replacements for conventional steel used for automotive body panels (Wagoner [10]). The lack of an accurate springback prediction is one of the principal obstacles to their widespread adoption.

Springback is the elastically-driven, but not purely elastic, change of shape of a sheet metal part upon unloading after forming (Wagoner [10]). Mostly these shape distortions are not accounted for beforehand at the stage of tooling design. Therefore an extensive experimental trial and error process has to be performed to determine the final tool design, choice of blank material and lubricant that will actually lead to the dimensionally accurate product (Meinders [7]). In addition the amount of springback can be reduced by means of different control techniques, such as, maintaining strong tensile forces in the deformed material, multi-step process, variation of the blank holder force during the forming process etc (Wenner [12]). With the wider use of high strength steels and various aluminum alloys in the automotive industry the springback problem becomes more unpredictable since the guidelines for conventional steels are not applicable anymore. This engenders a large reject of formed parts that are considered inadequate at the assembling stage.

The development and improvement of guidelines and software for the modeling of a certain forming process might significantly reduce the costs and the lead-through time from design to production of a product, by means of replacement of the experimental trial and error process, highlighted by a dashed rectangle in Figure 1, by a numerical one.
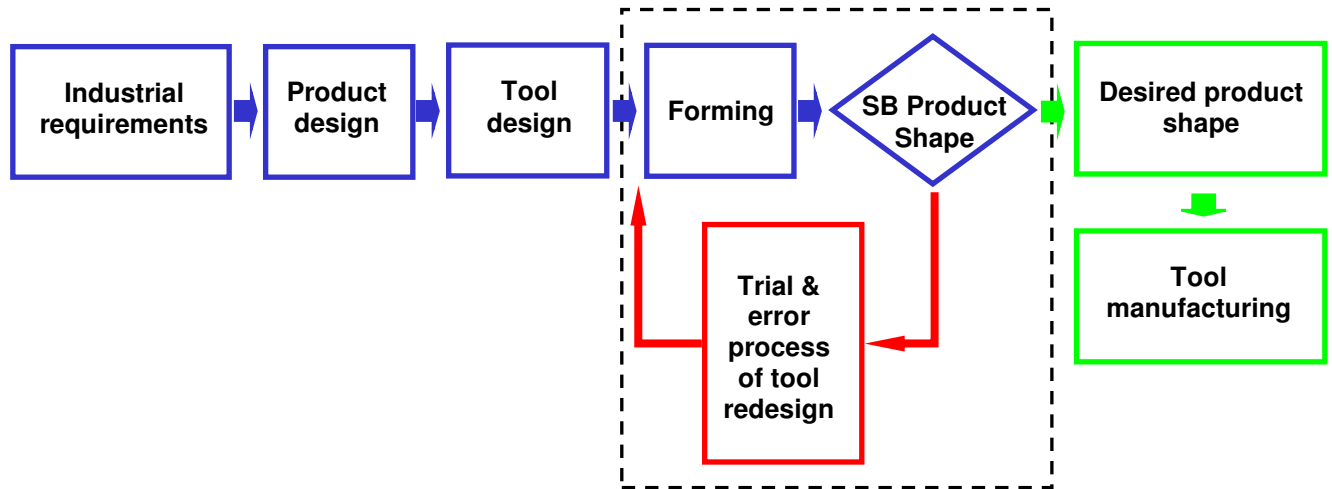
Figure 1: Sketch of the production procedure of an automotive part.

Springback simulation by the finite element method (FEM) has been attempted by various types of codes. The accuracy of a springback prediction depends on the accuracy of the stress state. The accuracy of the stress state is influenced by the many factors, such as constitutive equations, friction and contact behavior, tool surface discretization, the used element type, integration schemes, variation in material properties, mesh adaptivity and the solution algorithms of the system equations.

In case of multi-stage sheet metal forming operations (full process), physical phenomena, which appear in one process, can affect the sheet deformation in subsequent processes. This situation indicates that the history of sheet deformation must be taken into account if satisfactory results of full process modeling are expected. Real sheet metal production processes might comprise the following sequence of manufacturing operations:

- blanking
- stamping/deep-drawing
- cutting/trimming
- flanging
- hemming

All these operations contribute to the total springback of the final product. Geometrical defects accumulated during successive operations create problems at the assembling stage of the "fully" manufactured parts. These geometrical defects can be accounted for during tool modification by taking into the account the amount of springback shape distortion effects occurring after every forming operation.

To avoid the time consuming and expensive experimental tool alteration, the amount of springback after each forming operation must be numerically predicted as accurate as

possible and accounted for at the tool design stage, by means of springback compensation method (see e.g. Wagoner [11], Zimniak [14]). This kind of control of the springback phenomenon during full process modeling will enable tool designers to numerically evaluate the first design of the tools, and eventually to redesign dies to meet the growing quality demands of the automotive industry for the desired product shape.

In this report, the focus is on an accurate numerical description of the trimming operation after forming.

1.2   Trimming

The industrial manufacturing technology of most sheet metal parts comprises deep drawing and successive trimming (cutting) operations. Cutting operations involve separating two or more parts. Basically, metal cutting is a process where the material is sheared until it breaks, see Figure 2.
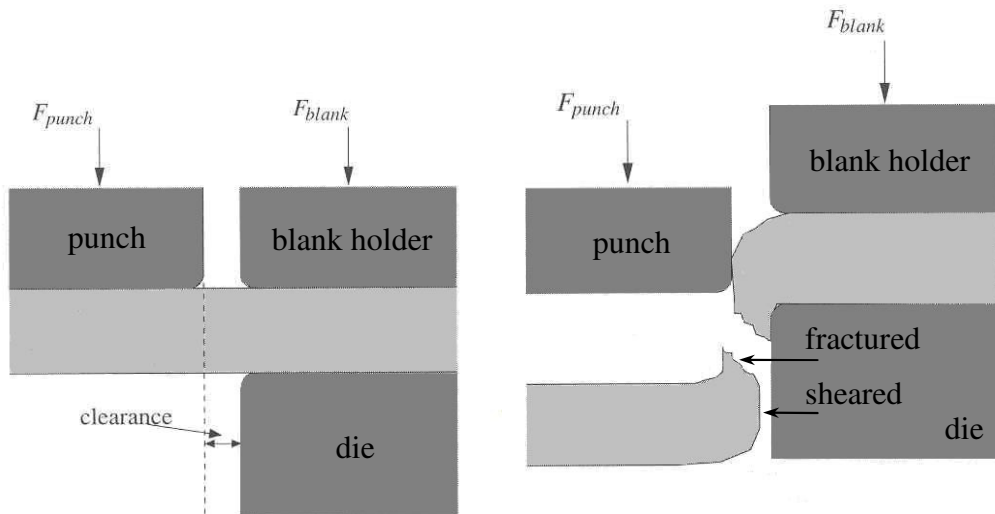
Figure 2: The cutting process.

The metal cutting process that is considered in this research is the shearing performed along the straight lines. Within the research described in this report a numerical trimming operation was developed. In Figure 3 the performance of the trimming algorithm is presented on an example of the real life product, an airplane wing leading edge stiffener. The pressed product is trimmed along a complex trimline prior to mounting it in the wing leading edge (Lamers [6]).

Figure 3: Wing leading edge rib after deep drawing and trimming.

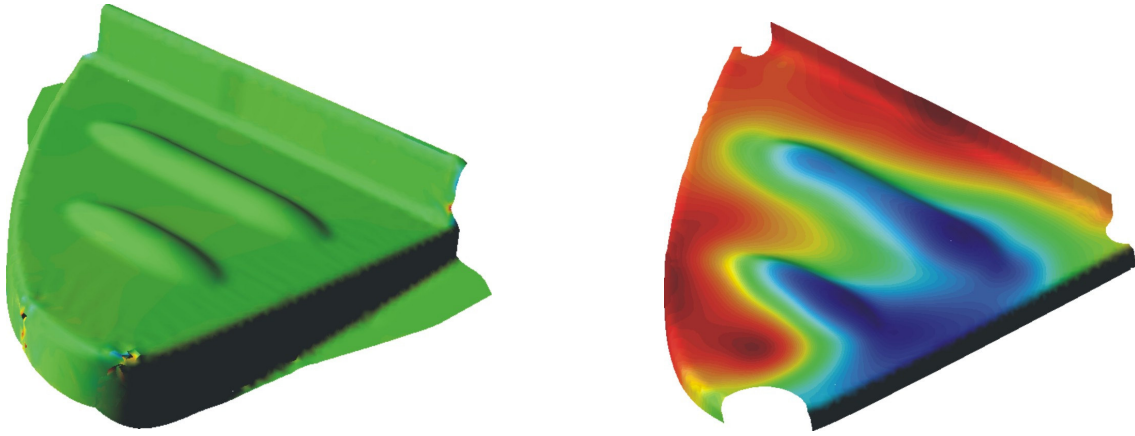Most researches in this field are concentrating on the cutting process itself rather then on the shape aberration of the product after it. The difficulty in simulating the springback and trimming operations was considered by Kawka [5] and Moesdijk [8].
This report discusses techniques that focus on the improvement of the predictability of the springback of the product after trimming. The accuracy of a springback prediction depends on the accuracy of the stress state. Therefore, the techniques mentioned above are developed in an attempt to capture the stress state situation after trimming as accurate as possible. Thereafter the main question has to be answered: "Does the accuracy of the stress state prediction after trimming significantly improve the springback behavior of the product?"
This is an interesting problem to investigate due to the fact that currently most commercial finite element codes, used by industry for solving the sheet metal forming problems, employ rather crude procedures for mesh and state variable data manipulations within trimming operation.
The calculations described in this report are performed with the Finite Element code DiekA.

1.3   Purpose and outline

The primary aim of current research is the improvement of numerical prediction of springback after trimming operation by means of development of accurate algorithms that accounts for the accurate stress state in the material. This research is one part of a global project within the framework of the Netherlands Institute for Metals Research (NIMR) entitled "Springback: improvement of its predictability to meet industrial requirements" (project number: MC1. 02121).

The complete numerical trimming operation consist of mesh adaptation to trimline and mesh improvement techniques and two techniques of taking into account the stress state change due to cutting. All these techniques are discussed in detail in the present report. The first data manipulation technique concentrates on the effect of the plate element mesh cutting and involves an accurate in-plane mapping of the state variables from the

formed untrimmed to the reduced trimmed mesh. The second technique incorporates the effects of the 2D (through the thickness) cutting process in the deep drawing or plate model. A mapping strategy has to be used for this purpose, since the 2D cutting operation is performed with continuum elements whereas the 3D deep drawing simulation makes use of shell elements.

This report is organized as follows. In Chapter 2, description of the numerical trimming process modeling is presented in general details. A brief description of finite element setup as well as the motivation for the element type choice for the numerical modeling is given. The mesh and the first stress state data manipulation technique (in-plane mapping) are discussed in Chapter 3. These techniques concern the improvement of the accuracy of capturing the actual in-plane stress state in the material after the trimming operation, which in fact improves the accuracy of a springback prediction. In Chapter 4 the second technique, the data transfer from 2D to 3D model, is considered. Chapter 5 presents and quantifies the numerical results illustrating the techniques discussed in the previous chapters. In order to quantify the amount of springback after trimming operation with and without mesh and data manipulation techniques several products are extensively studied, namely, a quarter of a rectangular and a circular cup, an S-Rail and a scaled-down car roof (Component 2 of the sensitivity analysis, performed within the springback project). For each product the springback behavior was studied when different trimming patterns were applied. Finally, in Chapter 6 conclusions of this study are drawn.

Numerical trimming operation

In order to be able to calculate the springback of the product after a forming operation, the residual stresses in the plate resulting from this process must be known. As was already mentioned before, one of the reasons for the inaccuracy in stress state prediction is an inaccurate simulation of trimming operation.

Meanwhile, the redistribution of internal stresses after the unloading of the sheet metal part is the only cause of the springback phenomenon after the forming stage, such as deep drawing. Trimming operation in its turn induces additional stress state change on the sheet metal. The force unbalance provoked by cutting off a part of a product material only aggravates the situation.

This chapter is organized as follows. First, a description of the numerical trimming process modeling is presented in general details as it was handled in studies preceding to the current research. Then, the motivation for the element type choice for the numerical modeling is given. And finally, a brief description of finite element setup is presented.

2.1 Numerical approach

The present report discusses techniques, which allow taking into account the stress state change due to the element mesh cutting, to improve the accuracy of the trimming simulation.

The problem of the numerical trimming operation is already studied in general details (Moesdijk [8], Zimniak[14]). It is analyzed as follows. In order to obtain the residual stresses in the product at the end of the process before springback, the part that is cut off must be removed from the mesh. Usually this is done by means of removing complete elements. When throwing away the elements, numerical equilibrium is no longer satisfied.

In general the elements are removed whether on inner or outer edge of the range of trimmed elements. Similar approach is usually implemented in commercial finite element packages, which results in trimmed edge crudely following the defined trimline, the line along which the trimming is performed, as shown in Figure 4.

The unequilibrated forces can cause numerical problems at the next stage of the simulation and therefore have to be balanced. The unbalance of the internal and external forces is cancelled by means of stepwise reduction.
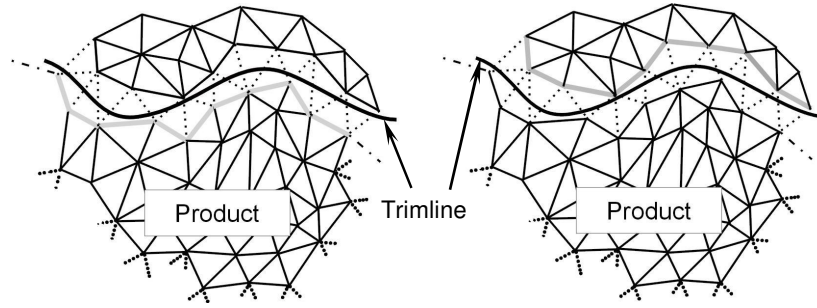
Figure 4: Removal of complete elements of cut off part along the inner (left) and along the outer (right) edge of trimmed elements.

As mentioned previously, current work concentrates on the improvement of the accuracy of numerical trimming procedure. The techniques adopted comprise stress state data manipulations as well as geometric mesh treatment. The latest involves mesh adaptivity procedure confirming the trimline, which allows, on the contrary to the analysis reported by (Moesdijk [8], Zimniak[14]), to perform such removal of elements that the trimmed edge of the resulting mesh closely follows the trimline. These techniques will be discussed in detail in Chapter 3. Since mesh manipulation is an important part of this study, the mesh element types available for sheet metal forming problems deserve a closer attention.

2.2 Choice of element type

The semi-finished products that subsequently are subjected to trimming operation are usually preformed by a number of stamping operations. During stamping or deep-drawing operations sheet metal is subjected to a very complex deformation history and boundary conditions. Some parts of the sheet deform under almost pure stretching, whereas other parts can develop significant bending strains. The deformation mode can be very complex in the parts of the sheet where severe bending or double-sided contact with tool exists. Therefore the theory needed to describe deformation in a sheet can vary from a two-dimensional (membrane assumptions) approach to a fully three-dimensional approach. Three distinct classes of elements used in the simulation of sheet metal forming processes are known: membrane, shell and solid.

Elements based on the membrane theory are the simplest ones. They are very efficient and cheap in simulation, but any results obtained by means of membrane elements suffer from a lack of the bending effects. Due to this fact, it is not possible to accurately simulate springback after a stamping or deep-drawing process when using only membrane elements.

Solid (continuum) elements are used to simulate sheet forming only in situations where fully three-dimensional theory is needed to describe the deformation process. Solid elements are difficult to employ in sheet forming analysis due to their far too stiff behavior in bending and problems with incompressibility condition. For complex sheet metal products it is not feasible to carry out a fully three-dimensional calculation.

Another alternative is the shell element. Such elements are usually used for simulations of structures, for which the thickness is very small compared to other dimensions, and therefore can be neglected. Unfortunately, not all shell theories are able to adequately represent the complex phenomena that exist in deformed sheets. But for purposes of deep-drawing and punching such shell theories, as Kirchhoff-Love and Mindlin-Reissner theories, have proven to give rather reliable results (Carleer [4]).

The element types usually used in the numerical analysis of sheet metal forming are:
MEM3D
2½D Membrane element (triangular) for the description of plate material, see Figure 5 (a). One integration point in plane and in thickness direction is used in this type of element. This element takes into account the membrane stresses. Every node has three displacements as degrees of freedom.

DKT3D
2½D Discrete Kirchhoff Triangle with three integration points in the plane and a variable number of integration points in thickness direction. This element takes into account the membrane stresses and the bending stresses. Every node has six degrees of freedom, three displacements and three rotations.

DST3D
2½D Discrete Shear Triangle with three integration points in the plane and a variable number of integration points in thickness direction. This element takes into account the membrane stresses, the bending stresses and transverse shear stresses. Every node has six degrees of freedom, three displacements and three rotations
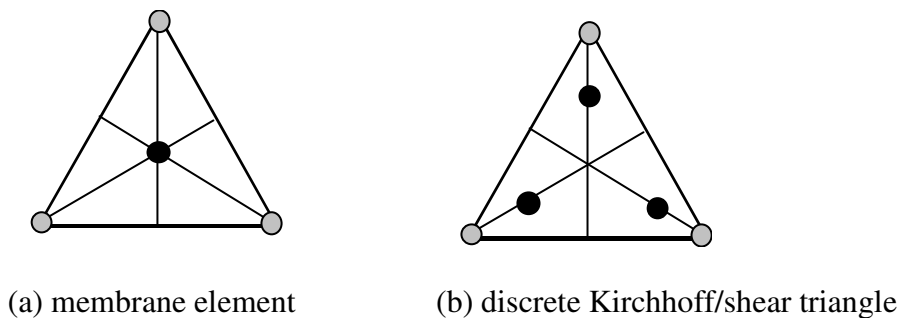

(a) membrane element   (b) discrete Kirchhoff/shear triangle

Figure 5: Location of integration points of a triangular element

In this research, the discrete shear triangle will be applied in the forming, unless mentioned otherwise. But when the stress state introduced through the thickness of the sheet by cutting operation itself is the subject of interest, 2D analysis has to be performed with bulk elements (rectangular element with four nodes and four integration points).

2.3   Finite element model

In this section the general model used for computations is presented. Where applicable, the feature of symmetry of the problem is exploited in an attempt of reducing the computational time. The blank holder, the punch and the die are modeled as rigid bodies. The blank material used for numerical analysis is the elasto-plastic (isotropic) Hill'48 with parameters summarized in Table 1.

E	v	R_0	R_{45}	R_{90}	C	σ_{yield}	n
210000 N/mm^2	0.3	1	1	1	550 N/mm^2	250 N/mm^2	0.22

Table 1 *The material parameters*

In order to describe the contact between the tools and the material of the blank, DiekA uses contact elements. Within this study attention was limited to normal contact behavior, known as the penalty approach, used together with Coulomb friction model. This model will be used in the forming, unless mentioned otherwise. The simulations are performed using a direct solver.

Mesh and data manipulations

In a forming process of real industrial components, excessive flange material left on the edges usually has to be trimmed off. When removing material, the change in stiffness may result in a different equilibrium shape.

In other words, in order to predict the product shape after trimming as accurate as possible one has to account for the residual stresses that were already present in the plate after deep drawing, the stress change due to the removal of a part of the material and the stresses induced on the cut edge by a plastic deformation of cutting process itself. Therefore, special techniques of mesh and data manipulation are necessary to include stresses originated due to cutting in the overall plate model.

This chapter covers the description of techniques called to improve the accuracy of the stress state prediction after trimming, thus the accuracy of the springback (Avetisyan [1]). First, the definition of trimming lines and planes will be given. The mesh manipulations, i.e. mesh adaptation to the trimline, will be addressed next. This involves a technique, which moves certain nodes of the element mesh to the trimline. Then, the procedure determining the part of the element mesh that will be kept (the product) after trimming by means of special data level structure is described. After mesh adaptation to the trimline, resulting element shapes might need to be improved, and this is done using a centering method. Finally, two data remap techniques are described, one of which is called to accurately map the stress state in-plane from untrimmed to trimmed and geometrically treated mesh, while the other data remap technique (2D to 3D) incorporates stresses induced on the trimmed edge of the plate by the cutting procedure itself into the full plate model.

3.1   Trimming lines and planes

The trimming algorithm developed within the current study gives the opportunity of numerical trimming of sheet metal parts described by shell element meshes. Currently the numerical cutting can be performed along the straight lines or along a whole collection of straight-line segments, referred to as a piece-wise linear trimline. The last option is employed in case the product needs to be trimmed along a curved line or an arc.

The algorithm responsible for the trimming operation within DiekA uses all information known after forming stage preceding to trimming, for instance the deep drawing stage.

The trimline information is entered into the model by means of creating a trimming plane or a number of trimming planes, which actually emulate the cutting tools (knives). In Figure 6 one such trimming plane is constructed on base of one straight timeline segment denoted *vec1* and a vector tangential to the surface of the cutting tool denoted *vec2*.

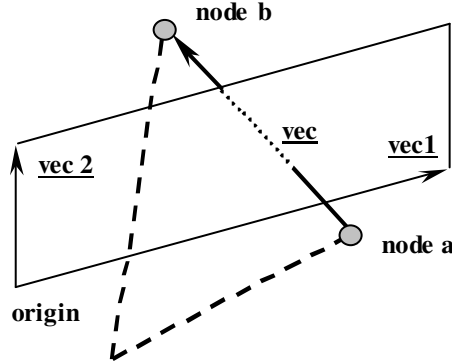**Figure 6:** Element side intersection by a trimming plane.

After the trimming planes are defined, the algorithm detects all cut through elements of the mesh. All three sides of every element are checked for an intersection with the trimming plane. In Figure 6 *node a* and *node b* define one side of an element, *vec*. The question, whether or not an element has an intersection with a trimming plane can be answered when solving equation (1) with respect to unknowns α, β and γ.

$$origin + \alpha\,\underline{vec1} + \beta\,\underline{vec2} = node\ a + \gamma\,\underline{vec} \qquad (1)$$

The element side has an intersection with a trimming plane if values of unknowns α and γ are between 0 and 1, whereas $\beta \in (-\infty, +\infty)$. The intersection point can be found using the following formula.

$$Intersection\ point = node\ a + \gamma\,\underline{vec} \qquad (2)$$

At this stage of the analysis when the intersected sides are known as well as the intersection points two nodes of each intersected side can be distinguished as the inner and the outer nodes with respect to the part that is kept as 'the product' after the trimming operation. It is done by choosing a *reference point* on the inside of the product and then performing an investigation similar to the one described in Figure 6, where the *node a* is substituted by the reference point and the *vec* (vector from *node a* to *node b*) is replaced by the vector normal to the trimming plane. After solving the modified equation (1), the parameter γ is kept as the *reference γ*. The sign of the *reference γ* then indicates the inside of the product. If γ found from equation (1) above has the same sign as the *reference γ* then the *node a*, of the intersected side, is considered to be situated on the inside of the product, while *node b* is outside.

3.2   Mesh adaptivity

Now the process of numerical trimming is looked at more profoundly. The issue of FE mesh disturbance (cut through of the elements), often neglected in commercial FE packages, enhances the internal stress change along the trimline and might have significant influence on the accuracy of the simulated springback. This is not of major concern for cases when the mesh is sufficiently fine. But due to the fact that the computational time is an aspect that nowadays retains high priority, trimming of the coarse meshes has to be performed as accurate as possible. In addition, usually, flat or shallowly curved parts are trimmed off, which in general are coarsely meshed.
In order to handle the mesh disturbance with respect to geometry and stresses, a mesh adaptivity technique has to be chosen and implemented. As an example, one such technique is illustrated in Figure 7, where an arbitrary mesh is adapted to the arbitrarily defined trimline.
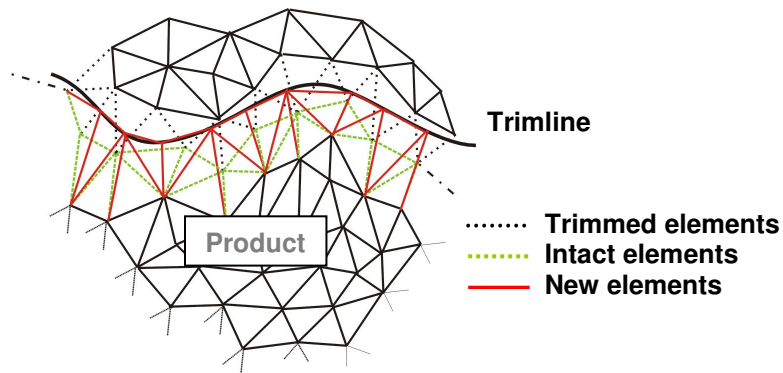

Figure 7: One alternative of mesh adaptivity

As can be seen in Figure 7, the nodes of the first row of the intact inner elements of the mesh are moved to the trimline perpendicularly, i.e. along the normal from the node in question to the trimline. The technique discussed above does not make use of the information obtained when defining the trimmed elements. The resulting geometric boundary of the product follows the trimline. However, the newly obtained elements are rather distorted and appear to be bigger than the rest of the elements of the mesh. This gives an idea about how much can the mesh be influenced by the adaptivity technique. Therefore, it is necessary to investigate a number of mesh adaptivity techniques in order to choose the one that produces a mesh with the best specifications.

Different methods adapting the mesh to a piece-wise linear trimline, such that exclusively inner and outer elements are formed were viewed. It must be noted that in all following methods the nodes of the trimmed elements are treated, i.e. moved to the trimline. Before node relocation two types of nodes are recognized in the trimmed elements, the inner and the outer nodes. The inner nodes are situated on the inner with respect to the trimline part of the mesh, which is kept after trimming and forms the 'product', while the outer nodes fall into the 'flange' part of the mesh on the other side of the trimline. The mesh adaptivity methods considered are:

1. Move outer nodes to the trimline perpendicularly
2. Move outer nodes to the trimline along the element side
3. Move inner nodes to the trimline perpendicularly
4. Move inner nodes to the trimline along the element side
5. Move combined method - nodes moved to the trimline perpendicularly
6. Move combined method - nodes moved to the trimline along the element side

In Figure 8 a node of a trimmed element is moved to the trimline in the first situation along the element side to the intersection point of the element side with the trimming plane, this kind of node relocation is used in methods 2, 4 and 6; and perpendicularly to the trimming line in the second situation for methods 1, 3 and 5.
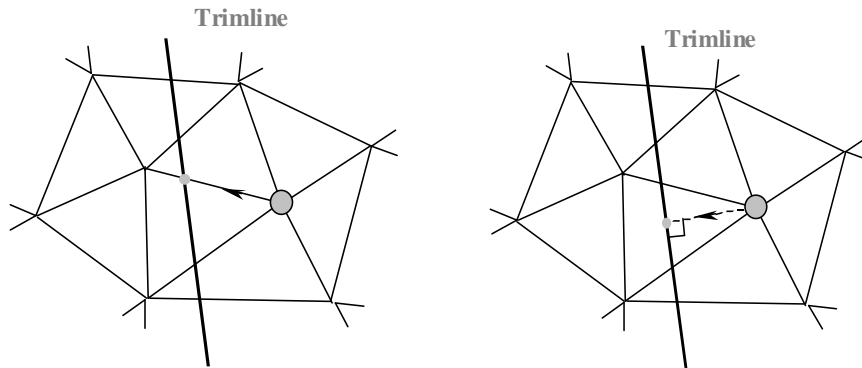

Figure 8: Node relocation to the trimline along trimmed element side (left) and perpendicularly (right).

When using the *Combined method* a decision must be made, which node to move to the trimline, whether the inner or the outer node of the trimmed side. It is expected that elements will be less distorted if the node closest to the intersection point of the trimline with the intersected element side will be moved.

All these methods were considered in as much detail as possible. The advantages and disadvantages of each with respect to mesh adaptation to the trimline are discussed below. Comparison between these methods is performed basing on the following main characteristics:

- Mesh quality after node relocation
- Level of difficulty of the method algorithm implementation.

Each of the above-mentioned methods was applied to the same mesh, which had to be adapted to a complex trimline. Performance of each method was discussed in 5 categories.

Category 1:   Elements turned inside-out

This phenomenon is explained in Figure 9. It occurs as an effect of node relocation and results in numerical problems because the turned inside out elements have negative area. An example is given in Figure 9: after relocation of the node *P* element 4 turns inside out.
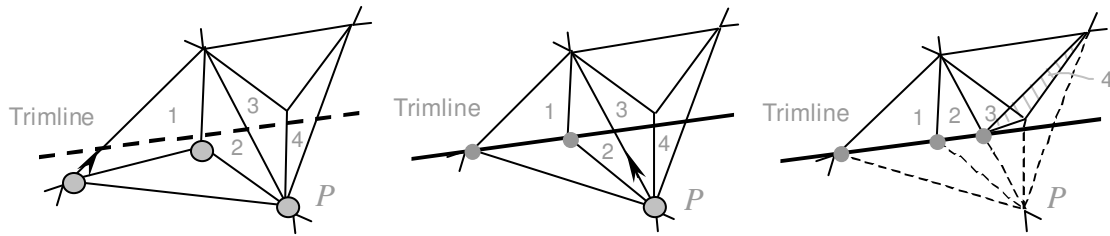
Figure 9: Node relocation causing element to turn inside out.

Category 2:   Distortion of the elements
The level of distortion of the elements is judged by their aspect ratio and the size of the newly formed elements in comparison with the average element size of the initial mesh.

Category 3:   Description of convexities of the trimline
Category 4:   Description of concavities of the trimline
Depending on the method of node relocation whether the concavities or convexities of the trimline can be poorly described, or both. For instance, when the method is based on relocation of the outer nodes, the convexity of the trimline (with respect to the product) can be underestimated while the concavity – overestimated. In case of relocation of inner nodes to the trimline the encountered situation can be exactly opposite.

The problem encountered when relocating nodes to the piece-wise linear convex or concave trimline (depending on which part of the mesh is kept after trimming as the product) is illustrated in Figure 10. By relocation of two nodes of element 3 to the trimline the corner made by two segments of the trimline is lost.
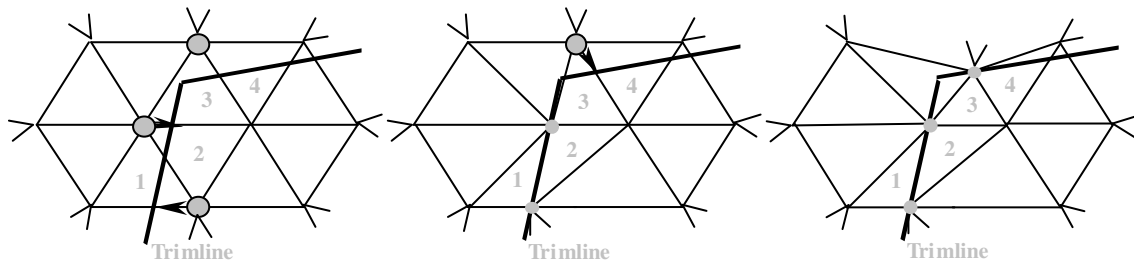

Figure 10: Lost corner in case of convex or concave trimline.

The problem of poorly described concavities and convexities is solved by Corner relocation procedure discussed in Section 3.5.

Category 5:   Level of the difficulty of the method implementation

All methods, using the node relocation tactic that moves nodes to the intersection point of the element side with the trimming plane, are easier to implement versus methods of perpendicular to the trimline relocation. In the latest the projection of the node in question on the trimline has to be found, whereas the information about all intersection points is available from the procedure described in Section 3.1.

In Table 2, the grading of the methods in all five categories is summarized, where '-' and '+'stand for the positive and the negative performance of a method respectively.

	Category 1	Category 2	Category 3	Category 4	Category 5
Method 1	-	-	+/-	-	-
Method 2	-	-	+/-	-	+
Method 3	-	+	-	+/-	-
Method 4	-	-	-	+/-	+
Method 5	-	+/-	+/-	+/-	-
Method 6	-	+/-	+/-	+/-	+

Table 2: Summary of performance of node relocation methods.

All of these methods encountered problem of the element turning inside out during node relocation. This problem is usually solved automatically during mesh smoothening, or centering, step that is discussed in Section 3.4. Another way (adopted in the method implemented within this research) of dealing with elements that have negative area, i.e. turn inside out, is to consider them to be outside of the mesh that is kept as the inside of the product, so that they do not contribute to the further analysis.

Basing on the results of the investigation of all six relocation methods presented in Table 2 the method of mesh adaptivity technique for the numerical trimming employed in the current study was chosen to be the "Combined method with nodes relocated to the trimline along the element side' (method 6). The node of the trimmed element side closest to the intersection point of the trimline with the intersected element side will be moved.

The *Combined method* was chosen because it produces the least distorted mesh. The node relocation along the element side is easier to implement due to the fact that the intersection points of the trimline with sides of all trimmed elements are already known. This method of node relocation performs well, but encounters one problem, when the nodes, movement of which is restricted by constraints of symmetry axes of the product, are treated. Such situation is illustrated in Figure 11. The node that belonged to the symmetry axis before mesh adaptation to the trimline leaves the axis.
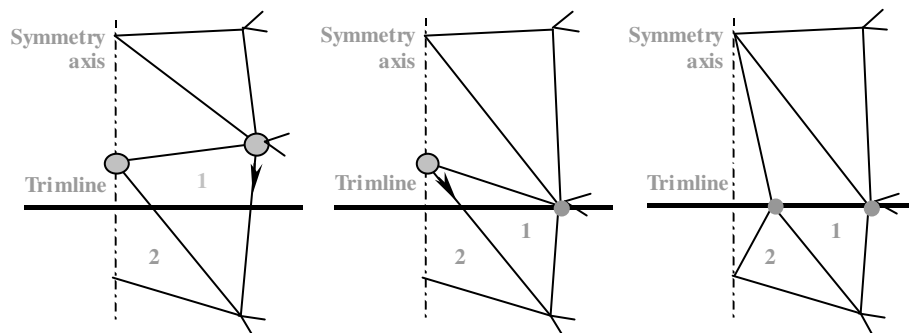

Figure 11: Problem of symmetry axis node relocation.

A special procedure was developed for treatment of these nodes. It recognizes the trimmed elements containing nodes laying on the symmetry axes and moves them to the intersection points of the axis with the trimline, as shown in Figure 12.
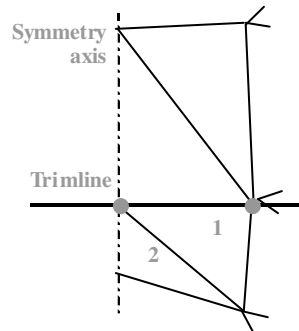

Figure 12: Relocation of the nodes belonging to the symmetry axis.

After subjecting the mesh to the chosen adaptation technique, elements will be already confirming the trimline.

3.3   Data structure for elements inside trimline

After node relocation to the trimline, such that exclusively inner and outer elements are formed, a *data level structure* was constructed, which indicates all nodes of the mesh whether as the inner or the outer with respect to the trimline. A schematic representation of node levels is shown in Figure 13.
The first step on the way of building up such data level structure is to look at all elements that have their nodes moved to the trimline, and tag these nodes as *level* 1 of the structure. At this stage nodes moved to the trimline are the only nodes of the entire (untrimmed) mesh that are labeled.
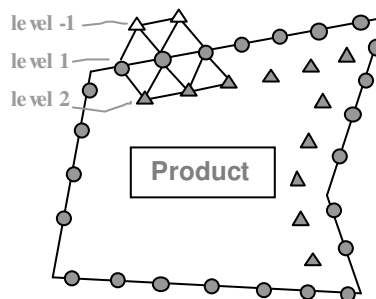

Figure 13: Node levels in data structure.

Next, all elements containing a tagged node are considered. For all such elements again use is made of the procedure described in Section 3.1, as mentioned for modified equation (1), but now the *node a* is substituted by the *node* that is not placed on the trimline and the *vec* is replaced by the vector normal to the trimming plane in question.

$$origin + \alpha\,\underline{vec1} + \beta\,\underline{vec2} = node + \gamma\,\underline{normal} \qquad (3)$$

When comparing the sign of γ obtained from equation (3) with the sign of the *reference* γ (see Section 3.1), which indicates the inside of the product, the *node* is labeled as *level* –1 (the outer level) in case of different signs of γ s and as *level* 2 (the first inner level) if they have the same sign.
Once this information is available the data level structure is built by a simple procedure. The elements containing *level* 2 nodes are looked at and the nodes of these elements that were not tagged yet are then labeled as *level* 3. This is done further inwards establishing a number of inside levels until no node is left on the inside of the product (trimline) unlabeled.

This kind of data structure appears to be very handy for the further analysis. An extensive use of the opportunities offered by the data level structure is made in the element improvement procedure described in the next section.

3.4   Centering method

Mesh manipulations, as described in the previous section, result in a, to some extent, disturbed mesh. The degree of disturbance depends on the quality of the original mesh and, of course, on the shape of the trimline. In some cases such geometric defects can spoil the accuracy of the springback prediction. In order to improve the shape and size of the elements node redistribution known as centering algorithm (Wisselink [13]) can be applied to the elements that were influenced by remeshing. The new coordinates of a node are calculated as the mean value of all coordinates of the neighboring nodes.

$$N_{new} = \frac{1}{i}\sum_i N_i \ , \ i- \text{ number of neighboring nodes} \qquad (4)$$
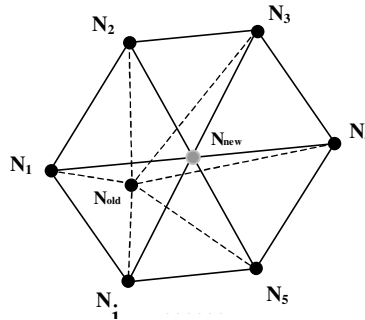

Figure 14: Centering method.

If applied to the nodes of *level* 1, i.e. the nodes placed on the trimline, the N_{new} is likely to be placed away from the trimline and therefore has to be projected back on the trimline.

The centering method does not treat the *level* 1 nodes and the nodes situated on the symmetry axes, such nodes retain their original nodal positions.

This smoothening procedure applied once to levels 2 and 3 provides a sufficiently regular mesh. But depending on the degree of element distortion after mesh adaptation technique it might be feasible to repeat the procedure.

3.5   Relocation of the corner nodes

In this section a solution to the problem of poor description of the corners made by the piece-wise linear trimline is discussed, see Figure 10. A procedure to capture the corner points of the trimline is developed. Within this procedure the information obtained in Section 3.1 by solving equation (1) is used. At each segment of the trimline the 0 and 1values of α indicate the beginning and the end of a segment, respectively. All nodes moved to the particular trimline segment have an α between these two values. The nodes with the smallest and the largest values of α for each segment is then found. At the corner where two trimline segments meet, the node closest to the corner is relocated to the corner, see Figure 15.
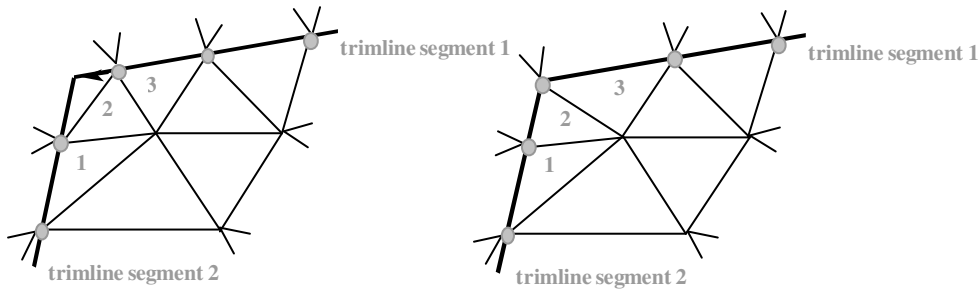

Figure 15: Relocation of a node to the corner of the trimline.

The corner relocation concludes the description of the geometric mesh manipulation procedures developed for the problem of numerical trimming considered in this research. The following two sections will cover the data mapping techniques that are necessary to obtain an accurate springback of the product. The problem of adaptive remeshing with data remapping (with convection) is the problem to be addressed next.

3.6   Data remap from the old to the new mesh

At the stage when the mesh is geometrically adapted to the trimline and treated by the centering procedure the elements close to the trimmed edge are altered to such extent that a new stress state for these elements has to be calculated. It must also be noted that due to node relocations the trimmed mesh might not be coplanar with the mesh prior to trimming. The accuracy of the springback simulation then will depend on an accurate in-plane state variable data-remapping algorithm from the old to the new mesh.

Two different methods of data remapping were viewed. The first method, in general details, comprised the following steps of data manipulation:

- Data extrapolation from old integration points (IP) to old nodes;
- Data averaging in each of the nodes of the given element over all neighboring elements;
- Interpolation of the data to the new integration points.

The other method involves:

- Projection of new integration points on the old mesh;
- Interpolation of the old data to each new integration point.

The first method mentioned above implies certain amount of smoothing. Therefore, preference was given to the second method. In addition, it is simpler to implement.

The general idea of the method is to interpolate the data known in the integration points of the untrimmed mesh to the integration points of the new mesh, which is adapted to the trimline. After the choice of the method is made, the data remapping algorithm can be developed in several steps.

First, positions of the new integration points in the new element mesh have to be determined. For a triangular element with three nodes and three integration points the use is made of the Gauss interpolation matrix N:

$$N = \begin{bmatrix} \frac{4}{6} & \frac{1}{6} & \frac{1}{6} \\ \frac{1}{6} & \frac{4}{6} & \frac{1}{6} \\ \frac{1}{6} & \frac{1}{6} & \frac{4}{6} \end{bmatrix} \qquad (x, y, z)^{new\,Nodes} \xrightarrow{\quad N \quad} (x, y, z)^{new\,IP's} \qquad (5)$$

Then, due to the fact that old and new meshes might be non-coplanar each new integration point has to be projected on the old mesh, see Figure 16.
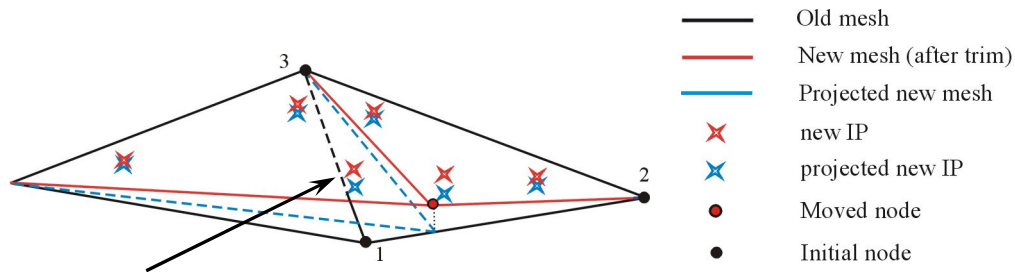

Figure 16: Correlation of the old and the new meshes.

Further analysis is based on the old element, in which the projection of the new integration point lies. It must be noted specially, that in the situation depicted in Figure 16, the new integration point (pointed at by an arrow) gets data from the topologically different element, i.e. element nodes of which are denoted 1, 2 and 3.

Thereafter, for all old elements containing the projection of the new IP's, the state variable data is extrapolated from old integration points to the old nodes. The use is made of the inverse of the Gauss interpolation matrix:

$$M = \begin{bmatrix} \frac{5}{3} & -\frac{1}{3} & -\frac{1}{3} \\ -\frac{1}{3} & \frac{5}{3} & -\frac{1}{3} \\ -\frac{1}{3} & -\frac{1}{3} & \frac{5}{3} \end{bmatrix} \qquad \zeta^{old\,IP} \xrightarrow{\quad M \quad} \zeta^{old\,Node} \tag{6}$$

This gives the opportunity to define the values of the state variables ζ (stress, strain, etc.) in the projection of the new integration point using the shape functions $L_i = A_i/A$ (A is the area of the complete triangle) built on the base of the old element, see Figure 17.

——	Old mesh
——	New mesh (after trim)
——	Projected new mesh
✕	new IP
✕	projected new IP
●	Moved node
●	Initial node
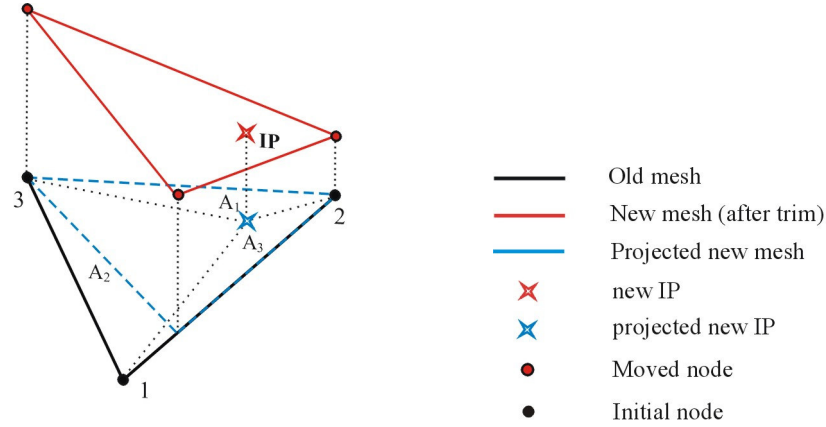
Figure 17: Contribution of the old element to data interpolation into the new IP.

In order to be able to use the interpolation functions, as described in Appendix A, the rotation (from 3D to 2D xy-plane) of every old element containing a projection of a new integration point is performed.

Finally, the values of the state variables known in old nodal points are used according to the following interpolation expression:

$$\zeta^{new\,IP} = \sum_{i=1}^{3} L_i \zeta_i^{old\,Node} \tag{7}$$

The values found are directly prescribed to the new integration point in the new mesh. This completes the calculation of the new stress state for each new integration point from the stress field of the old mesh.

Next, the state variable data manipulations concerning the incorporation of the stresses through the thickness of the plate introduced by the cutting operation will be in the focus.

Data transfer from 2D to plate model

The stresses implemented by cutting process itself due to plastic deformation in the thickness direction of the plate might have an effect on the springback behavior of the entire product. The internal stresses resulting from the blanking operation can be calculated with existing damage models. This is done by means of simulating a cutting process in 2D using bulk elements (many elements through thickness). When the internal stresses are known, these stresses can be applied at the integration points of the 3D model in the analogous way as was described in previous section for the in-plane data remap within the plate element mesh trimming process.
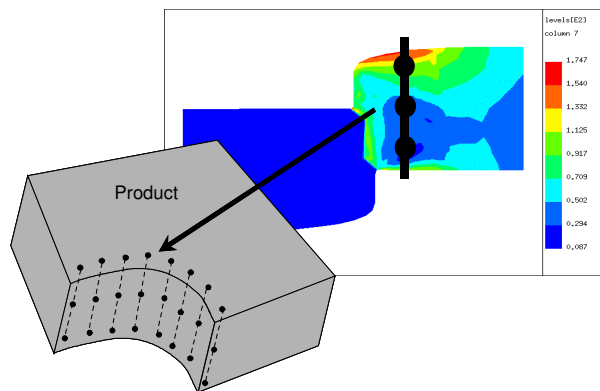
Figure 18: Incorporation of the 2D internal stresses (after cutting) in the plate model.

The investigation of the stress state transfer technique from 2D to 3D at the trimmed edge of the product is considered. The question to be answered is whether the accurate transfer of internal stresses, resulting from the blanking operation itself, to the trimmed edge of the plate, as shown in Figure 18, significantly influences the accuracy of a springback. It is known from literature that these stresses usually affect only a narrow band, three times the thickness of the plate wide, along the trimmed edge. In general, the shape of the whole sheet metal product is not expected to be largely influenced by the incorporation of this 'due to cutting' stress state data in the trimming model. But even if a small effect of these stresses will be observed in the amount of the springback after the trimming stage, one can expect it to be rather important at the next forming stages, such as the hemming stage, which, for example, is encountered in the car door manufacturing process. This operation is used for joining two automotive body sheet metal panels by bending the

flange of the outer panel over the inner panel. The unwanted springback after the trimming operation can lead to problems during the assembling. Therefore, all possible sources of stress change have to be investigated.

An algorithm that incorporates the effects of the 2D cutting process through the thickness (with bulk elements) in the deep drawing simulation of a complex product (3D) was developed (Avetisyan [2]). The procedure is schematically shown in Figure 19.
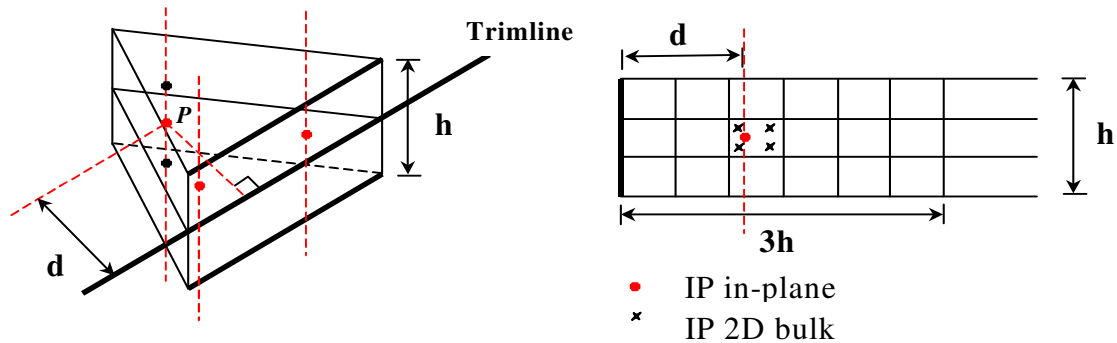

Figure 19: Data transfer from 2D to 3D.

The procedure comprises several steps. First, position of every integration point P in a triangular sheet element (1-3 points in-plane and 1-7 through the thickness, see Appendix B), which falls in a three thickness wide edge band mentioned before, is described by means of 2D coordinates (d, h). The coordinate d stands for the distance of the integration point from the trimming plane and h coordinate indicates the position of the integration point in the thickness direction. As was mentioned before, data to be mapped to these (d, h) points has to be obtained from 2D cutting simulation with bulk elements. In Figure 19 position coordinates (d, h) defined for integration point P, determine the element in 2D mesh, in which this integration point is positioned. The general idea is to interpolate the data from the quadrilateral element in question to the point $P(d, h)$.
This is achieved in a number of steps. The shape functions for a rectangular element with four nodes and four integration points (Figure 20) are defined as follows:
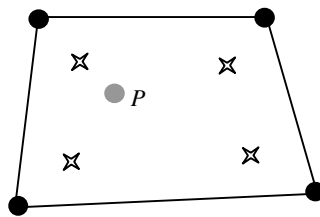

Figure 20: Rectangular element with four nodes and four integration points.

$$N_1 = \tfrac{1}{4}(1-\xi)(1-\eta)$$
$$N_2 = \tfrac{1}{4}(1+\xi)(1-\eta)$$
$$N_3 = \tfrac{1}{4}(1+\xi)(1+\eta)$$
$$N_4 = \tfrac{1}{4}(1-\xi)(1+\eta)$$
(8)

with the local coordinates $\xi, \eta \in [-1, 1]$. The integration points are located at the local coordinates $\left(\pm\tfrac{1}{\sqrt{3}}, \pm\tfrac{1}{\sqrt{3}}\right)$ (Gauss quadrature).

Step 1: Extrapolation of data from the IP's into the nodes of the rectangular element
In order to be able to perform this operation, by analogy with plate model remap, see (6), one needs the extrapolation matrix, which is an inverse of the interpolation matrix. In order to construct the interpolation matrix for a rectangular element with four nodes and four integration points we are substituting the coordinates of all integration points into the shape functions. The matrix obtained has the following structure:

$$N^{(4)} = \begin{bmatrix} a & b & c & d \\ d & a & b & c \\ c & d & a & b \\ b & c & d & a \end{bmatrix} \qquad (x, y)^{Nodes} \xrightarrow{\ N^{(4)}\ } (x, y)^{IP's} \qquad (9)$$

where

$$a = \tfrac{1}{4}\left(1+\tfrac{1}{\sqrt{3}}\right)\left(1+\tfrac{1}{\sqrt{3}}\right)$$
$$b = \tfrac{1}{4}\left(1-\tfrac{1}{\sqrt{3}}\right)\left(1+\tfrac{1}{\sqrt{3}}\right)$$
$$c = \tfrac{1}{4}\left(1-\tfrac{1}{\sqrt{3}}\right)\left(1-\tfrac{1}{\sqrt{3}}\right)$$
$$d = \tfrac{1}{4}\left(1+\tfrac{1}{\sqrt{3}}\right)\left(1-\tfrac{1}{\sqrt{3}}\right)$$
(10)

The inverse of the matrix $N^{(4)}$ is denoted as $N^{(4)}_{inverse}$.

$$N^{(4)}_{inverse} = \frac{1}{\det^4} \begin{bmatrix} a_1^* & a_2^* & a_3^* & a_4^* \\ a_4^* & a_1^* & a_2^* & a_3^* \\ a_3^* & a_4^* & a_1^* & a_2^* \\ a_2^* & a_3^* & a_4^* & a_1^* \end{bmatrix} \qquad \zeta^{IP} \xrightarrow{\ N^{(4)}_{inverse}\ } \zeta^{Nodes} \qquad (11)$$

where

$$a_1^* = a^3 + b^2 c + cd^2 - ac^2 - 2abd$$
$$a_2^* = -\left(d^3 + a^2 b + bc^2 - b^2 d - 2acd\right)$$
$$a_3^* = c^3 + ab^2 + ad^2 - a^2 c - 2bcd$$
$$a_4^* = -\left(b^3 + a^2 d + c^2 d - bd^2 - 2abc\right)$$
(12)

$$\det = aa_1^* + ba_4^* + ca_3^* + da_2^* \qquad (13)$$

Having the data in the nodes of the rectangular element in question it is possible to interpolate this data into the given point P, but first the local coordinates of this point in the bulk element have to be determined.

Step 2: Determining the local coordinates of the point P defined in the global coordinates. This step is described in detail within this report due to the fact, that unlike for the three node triangular elements, the expressions (transformation matrix) determining the local coordinates of the point positioned in a four node rectangular element were not found in literature.

The global coordinates of the point P can be described in global coordinates of the nodes of the element, in which it is situated, according to the expressions (14.a) and (14.b) for x and y coordinate respectively.

$$x_P = N_1(\xi,\eta)\,x_1 + N_2(\xi,\eta)\,x_2 + N_3(\xi,\eta)\,x_3 + N_4(\xi,\eta)\,x_4 \qquad (14.a)$$

$$y_P = N_1(\xi,\eta)\,y_1 + N_2(\xi,\eta)\,y_2 + N_3(\xi,\eta)\,y_3 + N_4(\xi,\eta)\,y_4 \qquad (14.b)$$

Substituting the expressions of the shape functions (8) in (14.a) and (14.b) we get the following expressions:

$$x_P = \tfrac{1}{4}\left[x_1^* + x_2^*\,\xi + x_3^*\,\eta + x_4^*\,\xi\eta\right] \qquad (15.a)$$

$$y_P = \tfrac{1}{4}\left[y_1^* + y_2^*\,\xi + y_3^*\,\eta + y_4^*\,\xi\eta\right] \qquad (15.b)$$

where the new coefficients are

$$x_1^* = x_1 + x_2 + x_3 + x_4 \qquad \text{and} \qquad y_1^* = y_1 + y_2 + y_3 + y_4$$

$$x_2^* = -x_1 + x_2 + x_3 - x_4 \qquad \text{and} \qquad y_2^* = -y_1 + y_2 + y_3 - y_4$$

$$x_3^* = -x_1 - x_2 + x_3 + x_4 \qquad \text{and} \qquad y_3^* = -y_1 - y_2 + y_3 + y_4 \qquad (16)$$

$$x_4^* = x_1 - x_2 + x_3 - x_4 \qquad \text{and} \qquad y_4^* = y_1 - y_2 + y_3 - y_4$$

The rearrangement of terms in the equation (15.a) gives an expression for ξ.

$$\xi = \frac{4x_p - x_1^* - x_3^*\eta}{x_2^* + x_4^*\eta} \qquad (17)$$

Substituting this expression into the equation (15.b) we arrive at the second order equation in η.

$$k_1\eta^2 + k_2\eta + k_3 = 0 \qquad (18)$$

where

$$k_1 = y_3^* x_4^* - y_4^* x_3^*$$

$$k_2 = -4y_p x_4^* + y_1^* x_4^* - y_2^* x_3^* + y_3^* x_2^* + 4y_4^* x_p - y_4^* x_1^*$$

$$k_3 = -4y_p x_2^* + y_1^* x_2^* + 4y_2^* x_p - y_2^* x_1^*$$

The two solutions to the equation (18) are:

$$\eta = \frac{-k_2 \pm \sqrt{k_2^2 - 4k_1 k_3}}{2k_1} \tag{19}$$

The solution we are interested in belongs to the interval $\eta \in [-1,\ 1]$. Substituting this value to the expression (17) we arrive at the local coordinates ξ, η of the point P. At this stage the shape functions can be constructed according to the expressions (8).

Step 3: After extrapolation of data into the nodes of the bulk element (step 1) and determining the shape functions based on the local coordinates of point P (step2) the state variable data can be interpolated into the point P as shown in (20).

$$\zeta^P = \sum_{i=1}^{4} N_i \zeta_i^{Node} \tag{20}$$

The direction of the calculated stress state in 2D model is different from that in plate model. Therefore, a transformation of these quantities has to be performed. The data transfer is concluded by rotation of the calculated stress state perpendicularly to the trimmed edge. For sheet metal forming, due to the general assumption that the normal stress and shear stresses action on the plane of the sheet are negligible, only three independent stress components remain.
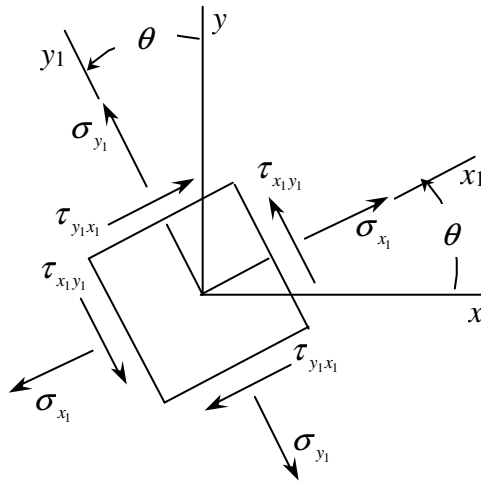
Figure 21: Two-dimensional view of an element in plane
stress oriented to the $x_1 y_1 z_1$ axes.

The following transformation rule applies:

$$\sigma_{x_1} = \sigma_x \cos^2\theta + \sigma_y \sin^2\theta + 2\tau_{xy}\sin\theta\cos\theta$$
$$\sigma_{y_1} = \sigma_x \sin^2\theta + \sigma_y \cos^2\theta - 2\tau_{xy}\sin\theta\cos\theta \qquad (21)$$
$$\tau_{x_1y_1} = -(\sigma_x - \sigma_y)\sin\theta\cos\theta + \tau_{xy}(\cos^2\theta - \sin^2\theta)$$

where $\sigma_x, \sigma_y, \tau_{xy}$ are the stresses calculated in 2D, $\sigma_{x_1}, \sigma_{y_1}, \tau_{x_1y_1}$ are the stresses transferred to the trimmed edge in the plate model and θ is the counterclockwise rotation angle of the $x_1 y_1$ axes with respect to the xy axes, as shown in Figure 21.

Finally, the rotated stresses introduced by the cutting operation are superimposed on the existing stress state of the plate model (due to forming process). The following procedure is pursued. First, the equivalent plastic strain of the 2D cutting operation $\varepsilon_{EQ}^{2D\,cutting}$ is superimposed on the equivalent plastic strain calculated on base of the strain state in the plate model ε_{EQ}^{plate}.

$$\varepsilon_{EQ}^{combined} = \varepsilon_{EQ}^{2D\,cutting} + \varepsilon_{EQ}^{plate} \qquad (22)$$

The combined equivalent stress can be calculated by the hardening law. In this report, use is made of the Ludwik-Nadai or Nadai relation (equation 23), which offers a good approximation of a large part of the true stress-strain curve (Boogaard [3]).

$$\sigma_{EQ}^{combined} = C\left(\varepsilon_{EQ}^{2D\,cutting} + \varepsilon_{EQ}^{plate}\right)^n \qquad (23)$$

Besides, not only the values, but also the directions of the stress states have to be superimposed. It has to be taken into account that a small change in deformation direction already dominates the combined deformation direction. Therefore a factor α is introduced to scale the cutting stress state with the forming stress state, in which this factor α depends on the elastic strain due to cutting.

$$\underline{\sigma}^{average} = \alpha\underline{\sigma}^{2D\,cutting} + (1-\alpha)\underline{\sigma}^{plate} \qquad (24)$$

where $\alpha = \dfrac{\varepsilon_{EQ}^{2D\,cutting}}{\varepsilon_{EQ}^{elastic} + \varepsilon_{EQ}^{2D\,cutting}}$ and $\varepsilon_{EQ}^{elastic}$ can be calculated from the 2D cutting stress state as follows:

$$\varepsilon_{EQ}^{elastic} = \frac{\sigma_{EQ}^{2D\,cutting}}{E}$$

For plastic cutting strains smaller than the elastic cutting strain, the influence of the stress state due to forming will dominate. However, for plastic strains larger than the elastic strain, the influence of the forming stress state will diminish fast, which means that the combined stress state will be dominated by the cutting stress state.

Then the average equivalent stress is calculated from the rotated cutting stresses obtained by (21).

$$\sigma_{EQ}^{average} = \sqrt{\tfrac{3}{2}\, \underline{\sigma}^{average} : \underline{\sigma}^{average}} \qquad (25)$$

By introduction of a scaling factor q (equation 26) it is possible to express the stress tensor $\underline{\sigma}^{combined}$ in terms of known quantities.

$$q = \frac{\sigma_{EQ}^{combined}}{\sigma_{EQ}^{average}} \qquad (26)$$

$$\left(\sigma_{EQ}^{combined}\right)^2 = q^2 \left(\sigma_{EQ}^{average}\right)^2$$

$$= q^2 \left(\sqrt{\tfrac{3}{2}\, \underline{\sigma}^{average} : \underline{\sigma}^{average}}\right)^2$$

Finally, the combined stress state is defined by:

$$\underline{\sigma}^{combined} = q \cdot \underline{\sigma}^{average} \qquad (27)$$

These superimposed values of the equivalent plastic strain and the combined stress state, defined by expressions (22) and (27), are returned to the plate model.

Applications

The influence of the two techniques of stress state updating after trimming on the amount of the numerical springback of the whole product, discussed in Chapters 3 and 4, is the major question to be answered in this report.
At the stage of the algorithm development for trimming, a rectangular cup was taken as a test problem.
Subsequently, the influence of the developed trimming techniques on the springback is investigated by means of trimming of a number of various products.
In Section 5.1 the general convention for representation of results presented in this chapter is given. Next, the reference simulation setup for the rectangular cup is presented in Section 5.2 together with simulations with variations in mesh size, plate thickness and tool radii. Section 5.3 discusses the results of trimming a circular cup. Thereafter Section 5.4 concentrates on the trimming of an S-Rail (Benchmark problem at the Numisheet '96). Finally, the amount of springback is looked at after trimming a scaled down car roof in Section 5.5. This product was simulated with two different materials, mild steel and high-strength steel.
A springback simulation can be performed in two ways, by gradual retraction of the tools or by a so-called instantaneous release. Due to the fact, that the method of gradual unloading is computationally costly, in most springback analyses the response of the sheet due to the release of the tools is numerically performed by means of instantaneous release, in one increment. Sometimes, this increment is subdivided into a number of sub-increments in order to avoid numerical instabilities. These occur because the contact forces are suddenly removed and transformed to residual forces. The sudden removal of residual forces can easily result in local buckling effects; hence the instantaneous release is sometimes done in a number of steps.
In all simulations, described in this chapter, the springback simulation after forming (deep drawing and/or trimming) stage is performed by an instantaneous release of the tools (if not mentioned otherwise).

5.1   General convention for representation of results

The figures presented in this chapter have a common agreement concerning the plotting of the results of the influence of different features of the trimming algorithm and of combinations of the mentioned techniques. The following plot arrangements hold if the

output for the quarter of a rectangular product, the quarter of the scaled down car roof and the quarter of a circular cup is discussed:

- The origin (cross section of both symmetry lines) is positioned on (0, 0, d), where d stands for the total punch displacement. The product is measured bottom down, see Figure 22 (a).

- Data along the symmetry lines is reported as a function of the current arc length, and runs from point C, via the origin, to point A, see Figure 22 (b) and (c).

- Data along the free edge is reported as a function of the current arc length, and runs from point A, via corner point B, to point C for the quarter of the rectangular cup and the scaled down car roof, see Figure 22 (b).

- Data along the free edge is reported as a function of the current arc length, and runs from point A along the bow-line to point C for the quarter of the circular cup, see Figure 22 (c).

- The results for the S-Rail are plotted along the vertical cross sections of the rail, as shown in Figure 22 (d).
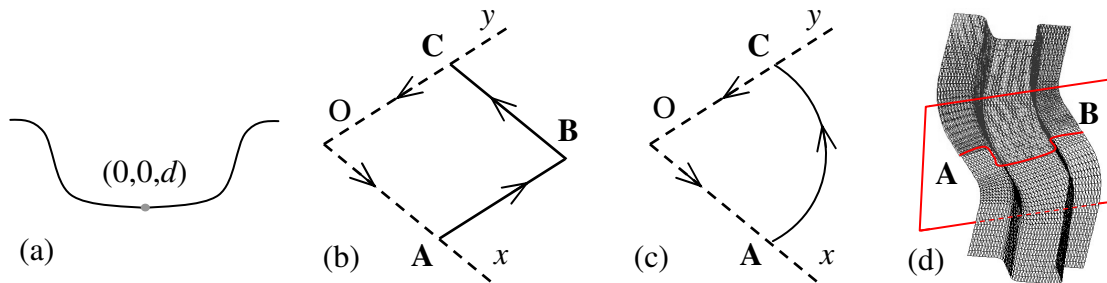
Figure 22: Convention of result representation for rectangular cup and the scaled down car roof, the circular cup and the S-Rail.

The formed and the sprung back patterns of the cross section (C-O-A) and flange (A-B-C) will be plotted under the legend entries:
legend entries:
- forming: the deformed product is still between the tools;
- sb_whole: the untrimmed product is allowed to springback.

The legend combinations for sprung back patterns after trimming with different techniques are:
- noc_nor: no centering or remap was performed during trimming;
- noc_r: during trimming remap was performed without centering;
- c_r: during trimming remapping and centering techniques were superimposed.

5.2   Rectangular product

To analyze the effect of the techniques discussed in the Chapters 3 and 4 a quarter of a rectangular deep drawn cup is now simulated with a 3D shell element model. The element type used is DST3D (3D Discrete Shear Triangle) with three integration points in the plane and five integration points in the thickness direction. This element takes into the account the membrane, the bending and the transverse shear stresses. Due to the restricted capacity of contemporary computers (with relation to computational time) and (double) symmetry of the product it is decided to simplify the FE model by means of imposing displacement boundary conditions on the symmetric planes (symmetry axes), i.e. a quarter of a rectangular cup is handled. The geometry of the rectangular tools and the blank are given in Figure 23. The product flange is positioned in xy-plane at $z = 0$. The punch stroke is -50 mm.
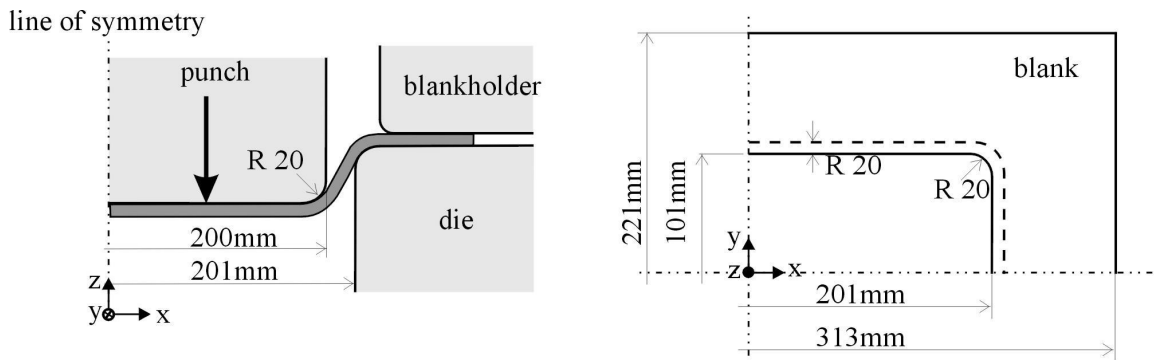
Figure 23: Tool geometry for rectangular cup.

If not mentioned otherwise a blank with a thickness of 1 mm is used. The blank material properties are listed in Table 3.
In this section, first, the effect of the mesh size variation on the amount of the springback obtained after trimming in combination with centering and remapping techniques will be discussed (see Subsection 5.2.1). The Subsection 5.2.2 will concentrate on the variation in plate thickness of the blank. And finally, the effect of the change in tool radii will be looked at in Subsection 5.2.3. In each subsection conclusions will be given, as well as for the complete Section 5.2.

Material properties		Process parameters	
E	210000 N/mm^2	punch displacement	50 mm
v	0.3		
σ_{yield}	250 N/mm^2	blank holder force	200 kN
C	550 N/mm^2		
N	0.22	coefficient of friction	0.16
R_0, R_{45}, R_{90}	1, 1, 1		

Table 3 *Properties of the rectangular cup deep drawing problem.*

5.2.1 Influence of mesh size

In order to study the effect of the mesh size on the amount of springback after deep drawing and trimming operations, this product was simulated with three different meshes. In the first mesh, the average element length is 10 mm, which means that the tool radii are rounded by 3 elements. This mesh will be referred to as *coarse mesh*. The second mesh has a typical element length of 5 mm – *medium mesh*, with 6 elements covering the tool radii. This mesh is considered to be the *reference* mesh for later study of the effect of variations in the plate thickness and the tool radii. The last mesh discussed for rectangular product is that having an average element length of 3 mm, i.e. 10 elements are describing the tool radius and the mesh is called *fine*.

In Figure 24 two representative trimlines cutting off a part of the quarter of a rectangular cup are shown. The *Trimline 1* refers to the piece-wise linear trimline (A*-B*-C*) approximating the corner of the 'product' obtained after trimming. Numerical trimming is performed by a number of trimming planes along the defined trimline. The *Trimline 2* (D-E) is obtained by trimming the deep drawn mesh by a horizontal plane coplanar to the *xy*-plane. The *Trimline 1* was applied to all three meshes mentioned above, while the trimming along the *Trimline 2* was performed only for the medium mesh.
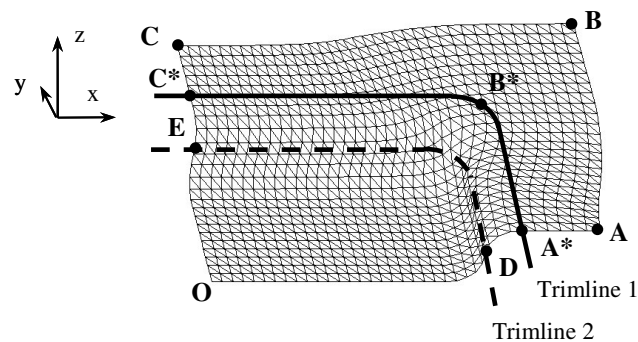
Figure 24: Quarter of the rectangular cup with trimlines.

Results for coarse mesh

Under consideration is a quarter of a rectangular product, simulated with coarse mesh with an average element length of 10 mm. This mesh is trimmed along the *Trimline 1*. The mesh reduced from 1200 elements to 703 elements during this operation, see Figure 25 (a).
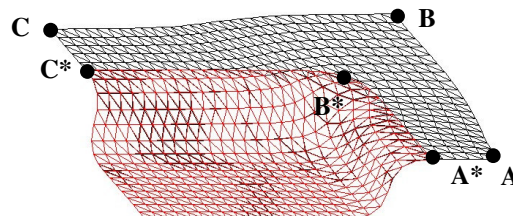
Figure 25 (a): Coarse mesh trimmed along the *Trimline 1*: formed (in black) and trimmed (in red).

The results of the springback simulations after forming are presented in Figure 25 (b). The formed and sprung back patterns of the complete/untrimmed flange (A-B-C) and trimmed flange (A*-B*-C*) are plotted under the legend entries described in Section 5.1. It must be mentioned that application of the centering technique within trimming operation to a mesh with radius covered only with 3 elements, resulted in diverging a springback simulation. The problem lies in the area of the algorithm deficiency. The centering, as it is implemented, is a procedure averaging the geometric position of all coordinates of the nodes falling under the category of nodes of *levels* 2 and 3 in the *data level structure*, as explained in Section 3.3. The *Trimline 1* is positioned such that mentioned node levels of the data structure for this coarse mesh are laying on the product curvature (tool shoulder). When the centering is performed the nodes 'penetrate the tool', due to the applied averaging. Therefore, a springback analysis becomes not possible (very likely, the equilibrium was too distorted).

Figure 25 (b) presents the deflection after springback of the flange of the whole product flange and the deflection of the flange of the trimmed product with and without remapping technique. All sprung back flange patterns show certain amount of buckling. This is the effect of compressive stresses, which are apparently present in some parts of the flange. The deflection of the untrimmed flange, from the *pressed flat – forming* pattern, ranges from –0.8 mm to 1.3 mm. When part of the blank material is removed by trimming operation the deflection range is reduced to –0.6 mm to 0.1 mm, which is within two thirds of the plate thickness. It can be explained by the fact that a part of the internal stresses guiding the springback is removed. In addition the trimmed flange lies closer to the product wall, therefore the amount of springback is influenced by the structural stiffness of the product.
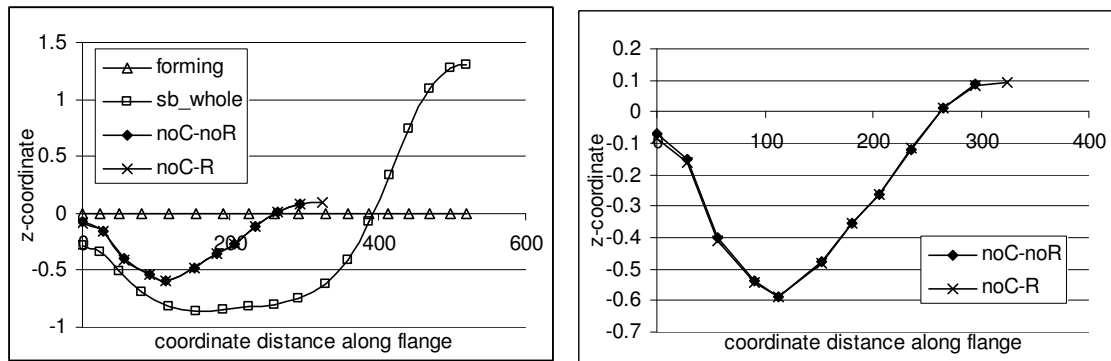

Figure 25 (b): Deflection of the flanges (A-B-C) and (A*-B*-C*) for coarse mesh.

The right plot of Figure 25 (b) only gives patterns of the sprung back flange after trimming with and without remap, which coincide up to 0.02 mm (maximum appears in the region 0-50 mm of the flange (A*-B*-C*)). When no centering technique is applied within trimming, the only element shape and size change takes place due to the geometric mesh adaptivity process to the defined trimline. In case of this particular coarse mesh the *Trimline 1* almost coincides with the element sides of most elements of the untrimmed

mesh treated by the mesh adaptivity procedure. Therefore, the distortion of most elements will be very small and the stress state change caused by the data remap from the old to the new mesh is negligible. As a result there is not much change in springback.

Next the shape along the symmetry lines of the product after forming and springback is focused on, see Figure 25 (c). The z-coordinate is given as a function of the arc length (Figure 22).
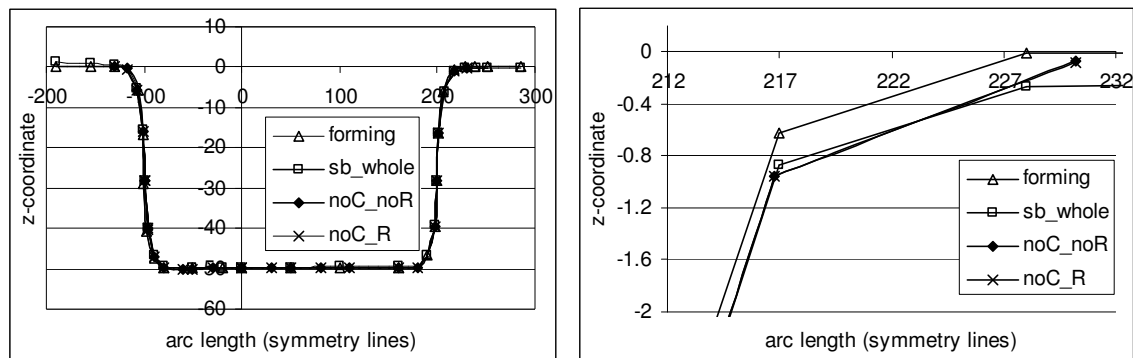

Figure 25 (c): Plate shape after forming along lines of symmetry (C-O-A) and
(C*-O-A*) for a coarse mesh.

In the left plot at –200 mm (point C) one can recognize the flange deflection of the whole product of magnitude of 1.3 mm and almost no difference in the plot patterns at 300 mm. This can also be explained by the structural stiffness of the product – point C is closer to the product shoulder than point A. The zooming in on the region 210-230 mm of the shape along the symmetry lines (Figure 25 (c), right) shows the coinciding springback patterns after trimming with and without remap as was reported previously. Note that the length of the element closest to the trimline has increased by 20 percent. In this case the new integration point of the elongated element will still be projected to the original element and will get data from the original element, from which it was formed. Therefore, the data remapping algorithm does introduce enough change in the stress field for a visible change in springback, compared to the springback after trimming without remap.

Results for medium mesh

Next the focus is on the same product simulated with medium mesh. The blank is meshed with 4800 elements having a typical element size of 5 mm, i.e. the tool shoulder is rounded with 6 plate elements. This mesh is trimmed along two trimlines: the *Trimline 1* and the *Trimline 2*.

Medium mesh trimmed along the Trimline 1

When trimming the medium mesh along the same *Trimline 1* (A*-B*-C*) that was applied to the coarse mesh, shown in Figure 24, the mesh reduces to 2822 elements, see Figure 26 (a).
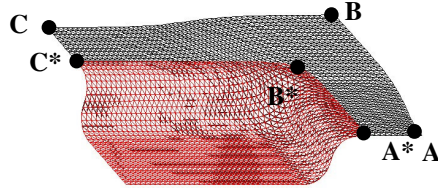

Figure 26 (a): Medium mesh trimmed along the *Trimline 1*: formed (in black) and trimmed (in red).

Figures 26 (b) and (c) illustrate the influence of the trimming algorithm on the amount of springback of this product, when the centering and remapping procedures are applied to the mesh in different combinations. The formed and sprung back patterns of the complete/untrimmed flange (A-B-C) and trimmed flange (A*-B*-C*) are plotted under the legend entries described in Section 5.1.

On the contrary to the coarse mesh, the application of the centering technique, within trimming operation, to the medium mesh was successful. This can be explained by the fact that the medium mesh contains smaller elements, so that the elements affected by the centering algorithm are positioned in a flat product area (die - blank holder region), coplanar to the *xy*-plane part of the flange. In this case no nodes are 'penetrating the tools'.
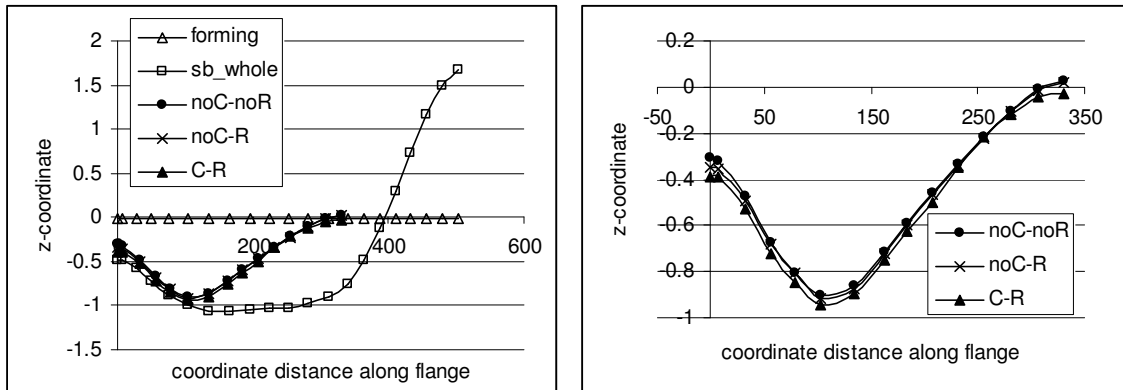
Figure 26 (b): Deflection of the flanges (A-B-C) and (A*-B*-C*) for medium mesh.

In Figure 26 (b) the same buckling behavior, as observed for springback of the coarse mesh, can be seen, whereas the deflection range in z-direction is somewhat different. The deflection of the untrimmed flange, referred to as legend entry *sb_whole*, shows its maximum of 1.7 mm at point C (see Figure 24) and minimum of -1.1 in the region 190-210 mm, which corresponds to the corner of the product, i.e. point B. The magnitude of the sprung back buckling pattern of the untrimmed medium mesh adds up to 2.8 mm, which is 0.7 mm larger than the same quantity observed for the coarse mesh. This is a noticeable effect of the springback simulation performed with a finer mesh.

Results shown in the right part of Figure 26 (b) correspond to the flange deflection patterns after trimming (A*-B*-C*). These patterns resemble the plots of the trimmed flange of the coarse mesh. The sprung back trimmed patterns vary from –0.95 mm to 0 mm. The range in simulation results is about the plate thickness.

In terms of the level of accuracy of the springback prediction after trimming all three plots of trimmed flange 'coincide', i.e. show insignificant differences for the overall product shape. Nevertheless, in terms of comparison of results obtained for the coarse and the medium meshes one can notice, that even though patterns noC_noR and noC_R mostly coincide, they show more deviation from each other than was observed in the similar plots for coarse mesh. It can be explained by the fact that for this particular mesh and trimline geometry, the new mesh obtained by the mesh adaptivity procedure is distorted in such a way that more integration points along the edge of the new mesh get their data from topologically different elements of the old mesh (see Figure 16, Section 3.6). The springback of the flange trimmed without centering but <u>with</u> remap is 0.025-0.05 mm bigger in regions 0-50 mm and 75-150 mm than that of the trimmed flange without centering and <u>without</u> remap. The application of the centering technique within trimming results in yet larger element shape and size change before remap and therefore, the superimposition of both techniques leads to 0.05 – 0.1 mm (5-10% of the plate thickness) more flange deflection than after trimming without centering and with- and without remap.

Next, under consideration is the shape along the symmetry lines of the product after forming and springback, see Figure 26 (c). The z-coordinate is given as a function of the arc length (Figure 22).

From Figure 26 (c) can be concluded that at points C and A the springback of the untrimmed flange measures 1.7 mm (actually spring forward situation – in the direction of positive z-axis) and 0.5 mm due to buckling, respectively.
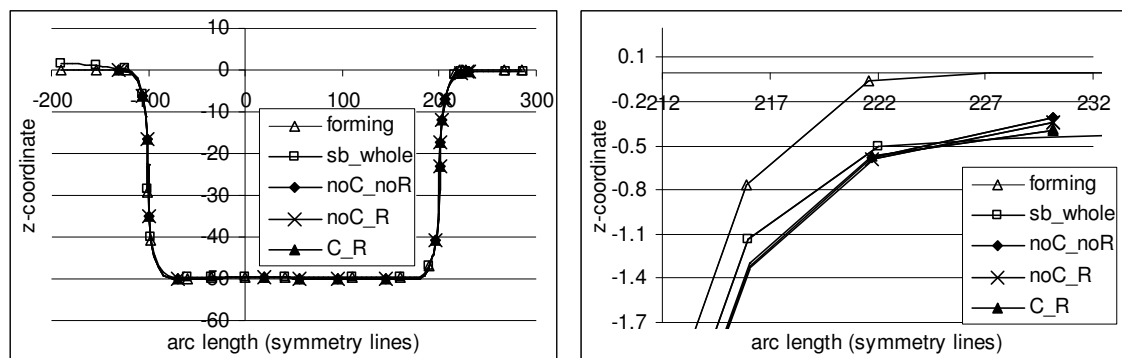

Figure 26 (c): Plate shape after forming along lines of symmetry (C-O-A) and (C*-O-A*) for a medium mesh.

The comparison of the trimmed flange deflection patterns with the untrimmed flange aberration reveals the difference in springback that is caused by the removal of the flange.

Zooming in on the region 210-230 mm of the shape along the symmetry lines (Figure 26 (c), right) shows <u>almost</u> coinciding springback patterns after trimming with- and without remap and centering. The only visible difference between these plots is observed in the

element on the edge. The springback after *noC_R* trimming is only 0.06 mm larger than the springback after trimming without application of the accuracy improving techniques. While the comparison of the patterns without both and with the superimposition of the techniques results in 0.15 mm (15% of the plate thickness) larger amount of springback in the later case.

Medium mesh trimmed along the Trimline 2

The results for trimming of the medium mesh along the *Trimline 2* are comparable to the results obtained for the *Trimline 1*, see Appendix C.1.

Results for fine mesh

Under consideration is the rectangular product simulated with fine mesh with an average element length of 3 mm, i.e. the tool shoulder is described by 10 elements. When this mesh was trimmed along the *Trimline 1* it reduced from 13068 elements to 7715 elements, see Figure 27 (a).
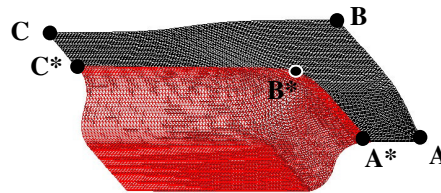
Figure 27 (a): Fine mesh trimmed along the *Trimline 1*: formed (in black) and trimmed (in red).

Figures 27 (b) and (c) illustrate the influence of the trimming algorithm, with springback prediction improving techniques, on the amount of springback of the rectangular product meshed with the fine mesh.
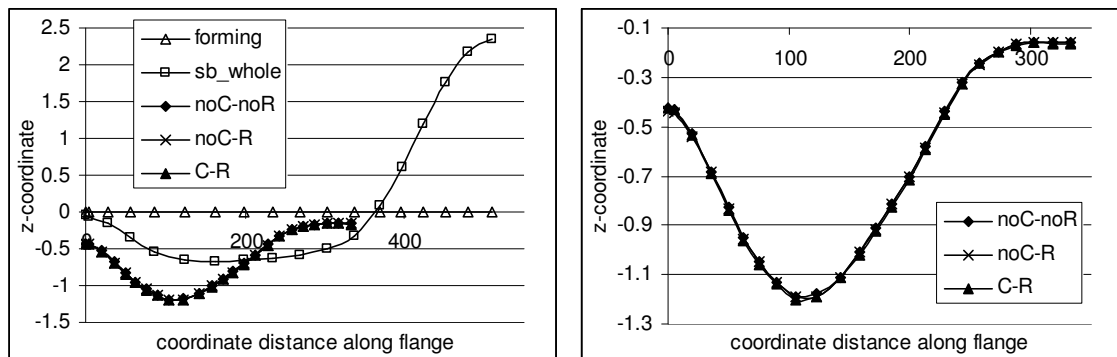
Figure 27 (b): Deflection of the flanges (A-B-C) and (A*-B*-C*) for fine mesh.

The tendency for the flange to buckle holds also for the simulations with fine mesh, as can be seen in Figure 27 (b). For the fine mesh the untrimmed flange deflection in

39

springback has a magnitude of 3 mm (three times the plate thickness), with minimum of -0.6 mm in the corner region and with maximum of 2.4 mm at point C, see Figure 22 (b). The sprung back flange plots after trimming with- and without remap and centering techniques coincide up to 0.02 mm in the corner region 90-110 mm of the flange (A*-B*-C*), with sprung back pattern after trimming with centering and remap giving this small deviation from the other two plots. This is an expected effect of application of mesh and data manipulation techniques to a very fine mesh. When the mesh is fine the techniques such as mesh adaptivity and centering are not changing the shape of the elements to such extent that the data remap from the old to the new mesh will significantly influence the stress state. In other words the data remapping algorithm will be mapping the data from the topologically same old element to the new one. Consequently the springback behavior after trimming will hardly be influenced by application of mentioned techniques.

The shape along the symmetry lines of the product after forming and springback, shown in Figure 27 (c), confirms the tendency for material at point C to spring forward. It shows a deflection of 2.4 mm. The right plot of Figure 27 (c), illustrates the springback, after trimming with- and without remap and centering, of the plate edge in *yz*-plane. As was mentioned in discussion of Figure 27 (b), all three sprung back patterns coincide due to the insignificant amount of geometric changes experienced by such a fine mesh during mesh adaptation to the trimline and during centering.
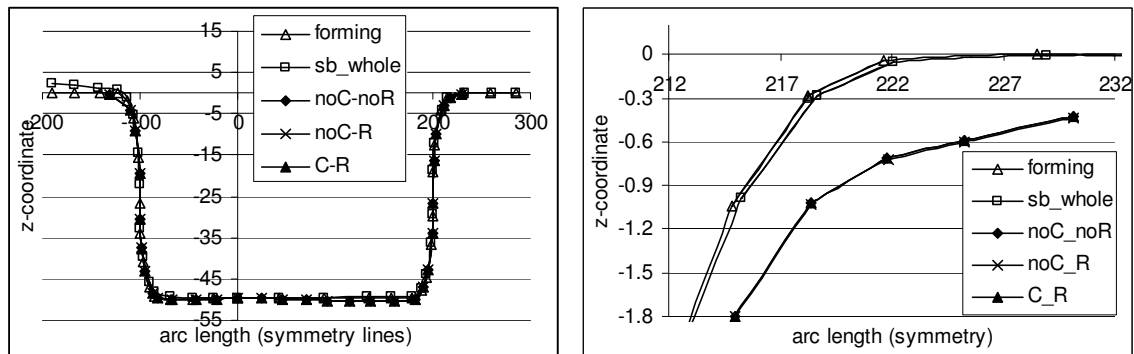
Figure 27 (c): Plate shape after forming along lines of symmetry (C-O-A) and (C*-O-A*) for fine mesh.

Conclusions for Influence of mesh size

Summarizing, the simulations of the drawing and trimming stages of a rectangular product, with- and without application of springback improving techniques in trimming, with three different meshes: *coarse, medium and fine*, have shown some similarities and some differences.

All sprung back patterns of the trimmed and the untrimmed flanges showed a tendency to buckle. The buckling behavior is driven by certain amount of compressive stresses in some parts of the flange.

With respect to the springback of the untrimmed mesh, the magnitude of the numerical springback increased with the decrease of the element size, with which the blank was meshed. When meshed with an average element length of 10 mm, the waviness in the flange measured about 2 mm. In case of a mesh with typical element length of 3 mm, the waviness of the flange after springback has a magnitude of 3 mm.

The application of data remapping technique results in larger springback for meshes that experience considerable geometric changes after trimming. In other words, the more integration points of the new elements get data from the topologically different elements of the old mesh, the larger the difference in springback will be, compared to a trimming simulation without remap. The extent of those geometric changes depends on the combination of the initial mesh size and the position of trimline. The coarser the mesh, the more geometric changes will be observed as a result of application of *mesh adaptivity to the trimline* and of *centering* methods. The degree of changes will be lower if the trimline 'roughly follows' the element sides of the mesh subjected to the trimming.

Quantitatively the springback after trimming with superimposed remapping and centering techniques results in up to 5-10% of the plate thickness larger springback than after trimming without application of mentioned techniques. A springback change of this magnitude can be considered as negligible.

5.2.2   Influence of plate thickness

In this section the effect of the plate thickness on the amount of springback after deep drawing and trimming operations will be discussed. The previous section, among others, described the results obtained for the trimming of the *medium* or *reference mesh* (average element length of 5 mm) with the blank thickness of 1 mm. In order to be able to make a fair comparison of the results with respect to the blank thickness, a new set of simulations was performed with the same mesh and process and material parameters but with different thickness, namely 0.7 mm.
The formed mesh is trimmed off along the *Trimline 1*, approximating the corner of the 'product' (A*-B*-C*) shown in Figure 24. During trimming operation the mesh reduced from 4800 to 2808 elements. It must be mentioned, that while having the same initial mesh of the thinner blank, the number of elements in the resulting mesh after trimming reduced in comparison to the same number for the mesh with thickness of 1 mm.

Figures 28 (b) and (c) illustrate the influence of the trimming algorithm, with springback prediction improving techniques, on the amount of springback of the rectangular product simulated with blank thickness of 0.7 mm, which is meshed with the medium mesh.
The flange shows the same buckling pattern as did flanges of all previous examples discussed. The deflection of the untrimmed flange (legend entry *sb_whole*) ranges from –0.2 mm to 2.8 mm. The magnitude of the sprung back buckling pattern adds up to 3 mm, which is 0.2 mm larger than the same quantity for the medium mesh with the blank thickness of 1 mm. In addition one can observe the fact that the sprung back patterns for

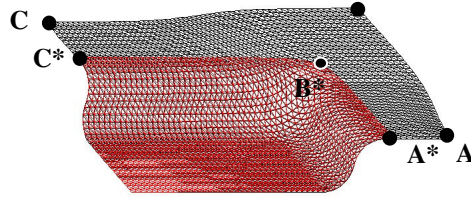the 0.7 mm blank lay 1 mm higher than that observed for the 1 mm *medium* meshed blank (see Figure 26 (b), left).

Figure 28 (a): Medium mesh, with plate thickness of 0.7 mm, trimmed along the *Trimline 1*: formed (in black) and trimmed (in red).

Results shown in the right part of Figure 28 (b) correspond to the flange deflection after trimming (A*-B*-C*). The sprung back trimmed patterns vary from 0.2 mm to 1.2 mm. The range in simulation results is within the plate thickness and, in terms of the level of accuracy of the springback prediction, all three curves 'coincide', which was also the conclusion in case of the *medium* mesh with 1 mm thick blank. But this is not the only similarity between the two. The comparison of deflected flange patterns after trimming with- and without centering and remap, when compared to each other, crop identical results to the ones obtained for the medium mesh with 1 mm thick blank.
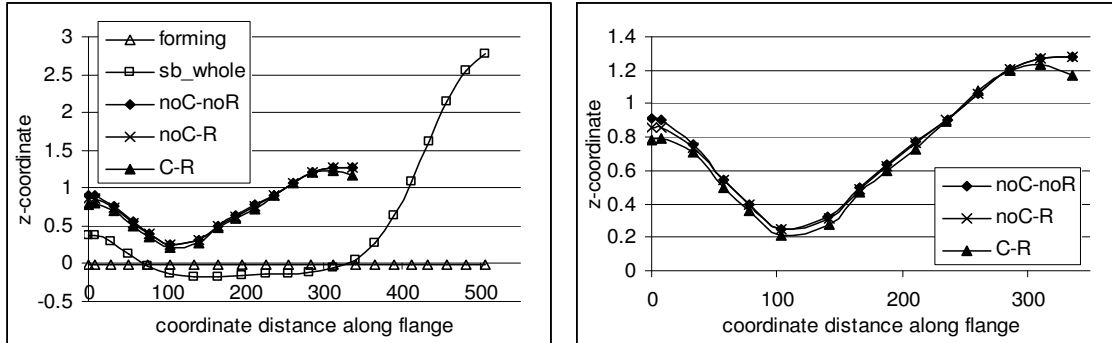
Figure 28 (b): Deflection of the flanges (A-B-C) and (A*-B*-C*) for medium mesh with plate thickness of 0.7 mm.
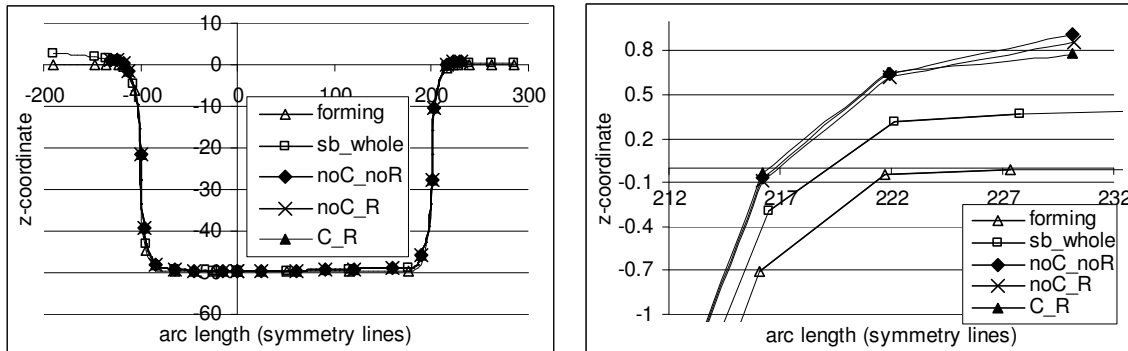
Figure 28 (c): Plate shape after forming along lines of symmetry (C-O-A) and (C*-O-A*) for medium mesh with plate thickness of 0.7 mm.

42

Conclusions for Influence of plate thickness

All three sprung back flange patterns, after trimming with various combinations of mentioned techniques, show similar deflection patterns and rates, compared to each other, that were observed for the default mesh with plate thickness of 1 mm. However, the magnitude of this deflection is bigger - within 1.4 times of the plate thickness and the patterns lay 1.2 mm higher. Quantitatively, the difference in springback after trimming results for given blank measures up to 7-14% of the plate thickness.

5.2.3   Influence of tool radii

This section discusses the effect of the tool radii on the amount of springback after deep drawing and trimming operations. The rectangular product discussed in previous sections was formed using tools, as described in Figure 23. In present section the focus will be on the product simulated with the same tool geometry but with tool radii of R=10 mm, instead of 20 mm. If the blank mesh will be taken such that the tool radii are rounded by 6 elements, which in this case means that the typical element length is 2.5 mm (Note: this is the finest mesh discussed for the rectangular cup), it will be possible to compare this results with the results described in Section 5.2.1 for the *medium* or *reference mesh* (average element length of 5 mm). The formed mesh is trimmed off along the *Trimline 1* (A*-B*-C*) shown in Figure 24. During trimming operation the mesh reduced from 19200 to 11998 elements.
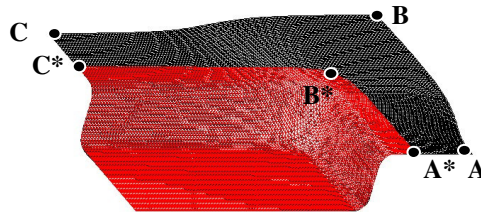
Figure 29 (a): Mesh, formed by tools having shoulder radii of 10 mm (with 6 elements on the shoulder), trimmed along the *Trimline 1*: formed (in black) and trimmed (in red).

Figures 29 (b) and (c) illustrate the influence of the trimming algorithm, with and without the techniques of centering and data remap, on the amount of springback of the rectangular product simulated with tools with shoulder and corner radii of R=10 mm. The flange (A-B-C) of the product in Figure 29 (b), the legend entry *sb_whole*, shows the same buckling pattern as the flanges of all previous examples discussed. It can be observed that the sprung back pattern of the untrimmed product lies at the same level as the similar graph of the fine mesh (see Figure 27 (b)) but with smaller magnitude. The deflection of the untrimmed product is such that the flange displacement in *z*-direction ranges from –0.75 mm to 0.55 mm. The magnitude of the sprung back buckling pattern adds up to 1.3 mm, which is more than two times smaller than the same quantity observed for the reference mesh with the tool radii of 20 mm. This is an effect of smaller

tool radii; the deep drawn product, obtained with R=10 mm radii tools, has a higher structural stiffness.

The sprung back trimmed patterns range from -0.35 mm to 0.3 mm and coincide up to 0.002 mm. It can be seen in the right part of Figure 29 (b) corresponding to the zoom-in on the region 220-340 of the flange deflection patterns (A*-B*-C*) after trimming. This result is consistent with the results reported earlier (see Figure 27(b), results for the fine mesh) and confirms the fact that in case of fine meshes the shape change due to the mesh adaptivity after trimming and due to the centering method is so small that the in-plane data remap algorithm hardly influences the springback of the trimmed product. Quantitatively, the difference in springback patterns after trimming with and without centering and remap for this particular mesh is only 0.2 % of the plate thickness.
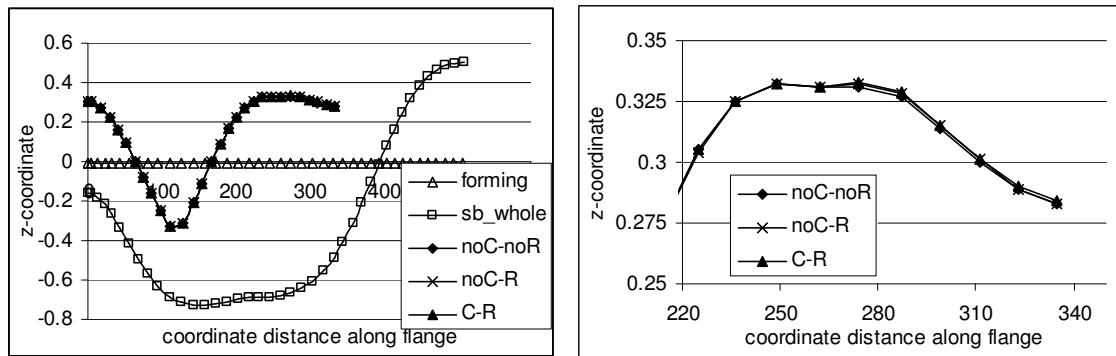
Figure 29 (b): Deflection of the flanges (A-B-C) and (A*-B*-C*) for mesh formed by tools having shoulder radii of 10 mm (with 6 elements on the shoulder).
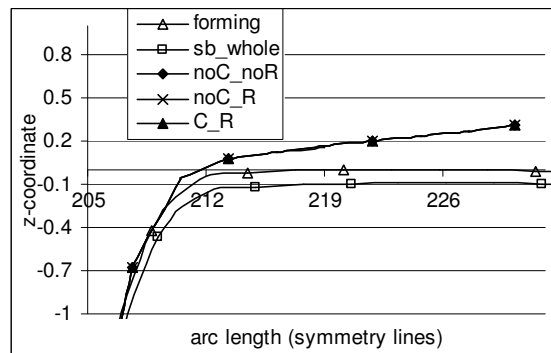
Figure 29 (c): Zoom-in on the plate shape after forming along lines of symmetry (C-O-A) and (C*-O-A*) for mesh formed by tools having shoulder radii of 10 mm (with 6 elements on the shoulder).

Conclusions for Influence of tool radii

With respect to the springback of the untrimmed flange, the tendency, for the increase in the amount of numerical springback with the decrease in mesh size observed in the previous study of mesh size influence, was not recognized for the present results. Although, the blank is meshed with 2.5 mm elements, the untrimmed mesh showed two

times less springback than the default mesh with 5 mm elements. This can be explained by the dominating effect of the structural stiffness of the product simulated with the tools shoulder and corner radii of which are R=10 mm. In addition, smaller tool radius introduces more tensile stress in plate, hereby reducing the springback.

The choice of the number of elements rounding the tool radii, made for the presented simulation, has predefined such a fine mesh that the methods of mesh and data manipulation (data remap) are not changing the stress state to such an extent that the data remap from the old to the new mesh will significantly influence the amount of the resulting springback. Quantitatively, the difference in springback patterns after trimming with and without centering and remap for this particular mesh is only 0.2 % of the plate thickness.

Conclusions for rectangular product

Summarizing, all sprung back patterns of the trimmed and the untrimmed flanges showed similar buckling tendency. The buckling behavior is driven by a certain amount of compressive stresses in some parts of the flange.

With respect to the springback of the untrimmed mesh, the magnitude of the numerical springback increased with the decrease in element size, with which the blank was meshed.

The application of the in-plane data remapping technique results in larger springback for meshes that experience considerable geometric changes after trimming with mesh adaptation and centering techniques. The extent of those geometric changes depends on the combination of the initial mesh size and the position of trimline. The coarser the mesh, the more geometric changes will be observed.

The magnitude of the numerical springback appears to be higher for thinner blanks. The product simulated with a thinner material has a lower structural stiffness, thus larger springback.

When the product is simulated with tools with smaller radii, the springback is dominated by the effect of the structural stiffness of the product. The halving of the radii results in more than two times smaller amount of the numerical springback.

Quantitatively the springback after trimming with superimposed remapping and centering techniques results in up to 5-15% of the plate thickness larger springback than after trimming without application of mentioned techniques. A springback change of this magnitude can be considered as negligible.

5.3   Circular product

Next, several other products will be trimmed with application of different combinations of developed trimming accuracy improving techniques. The ultimate goal is to find out if the tendency and the magnitude of the in-plane remap influence hold also for products with different geometry.

The following product to be analyzed is a circular cup. Analogously to the rectangular product, only a quarter of a circular cup is handled. The element type used is DST3D with three integration points in-plane and five integration points in the thickness direction. The blank is meshed by 7079 elements, with elements having a typical element size of 5 mm. The geometry of the circular tools and the blank are given in Figure 30. The product flange is positioned in xy-plane at $z = 0$. The punch stroke is -50 mm and the blank thickness is 1 mm.
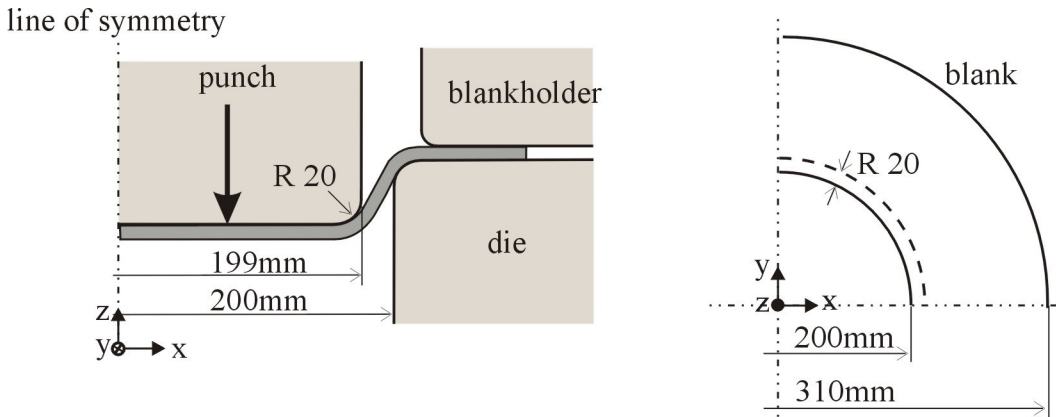
Figure 30: Tool geometry for circular cup.

The blank material and process properties are the same as used for the rectangular cup and are listed in Table 3 (see Section 5.2). In Figure 31 two trimlines cutting off the flange of the quarter of a circular cup are shown.
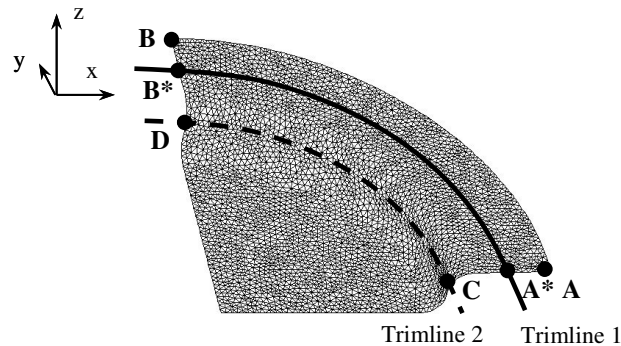
Figure 31: Quarter of the circular cup with trimlines.

In this section, the influence of the centering and in-plane data remapping techniques on the amount of springback obtained after trimming will be discussed with respect to the

mentioned trimlines. Subsection 5.3.1 will concentrate on the results concerning *Trimline 1*. This trimline refers to a piece-wise linear trimline (A*-B*) approximating the corner curvature of the product. Second trimline (C-D) is obtained by means of removing a bigger part of the product by a horizontal plane coplanar to the *xy*-plane, passing through the wall of the product. Results obtained for the second trimline are comparable to the results presented for the *Trimline 1* and can be found in the Appendix C.2.

Circular cup trimmed along the Trimline 1

Under consideration is a circular cup formed by tools specified in Figure 30. During trimming along the *Trimline 1* the mesh reduced to 5337 elements, see Figure 32 (a).
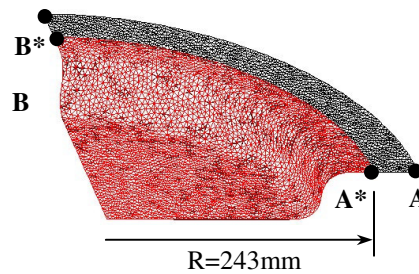
Figure 32 (a): Circular cup trimmed along the *Trimline 1*: formed (in black) and trimmed (in red).

The results for the springback after deep drawing and trimming are presented in Figure 32 (b), in form of flange deflection plots as was described in Figure 22 (c). In addition to all the flange position patterns mentioned in Section 5.1, the *z*-coordinate of the untrimmed flange is plotted along the arc (A*-B*) with R=243 mm radius, as shown in Figure 32 (a), which corresponds to the position of the *Trimline 1* approximating the corner curvature of the product.
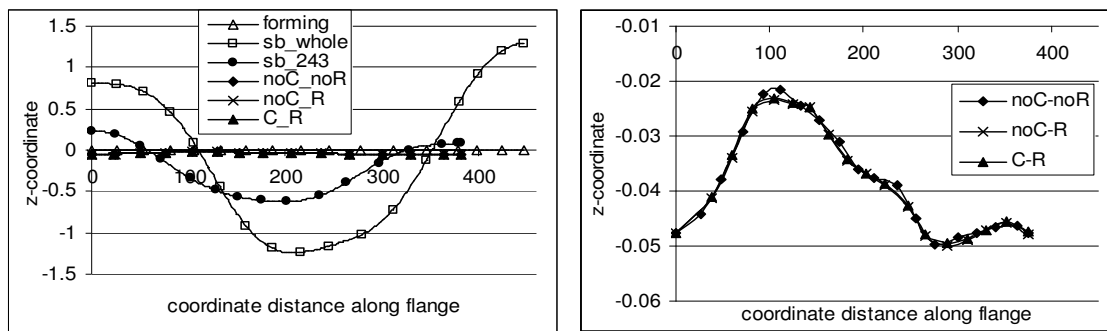
Figure 32 (b): Deflection of the flanges (A-B) and (A*-B*) for circular cup (*Trimline 1*).

All plotted patterns show a tendency to buckle. It is most visible for the complete untrimmed flange deflection (legend entry *sb_whole*), with magnitude of 2.5 mm, and for the deflection of the trimline arc level of the untrimmed mesh (legend entry *sb_243*), the amount of deflection of which adds up to 0.75 mm. The right graph of Figure 32 (b) zooms on the patterns of the flange after trimming and springback. When removing a part

47

of the flange, one ends up with the trimmed flange deflection of magnitude of 0.03 mm, which is a negligible amount. This can be explained by the effect of even higher stiffness of the circular cup compared to the rectangular product, so that when the stresses present in the flange are removed, this effect dominates the springback behavior. The application of the superimposition of centering and remap results in 0.02% of the plate thickness change of the amount of springback. This amount is smaller then the similar measure reported of the rectangular cup (5-10% of the plate thickness), even though the same element size was employed.

Figure 32 (c) shows the deflected product shape along the symmetry lines for the performance of the various algorithms. Again, it can be seen that the influence of the different mapping techniques is insignificant.
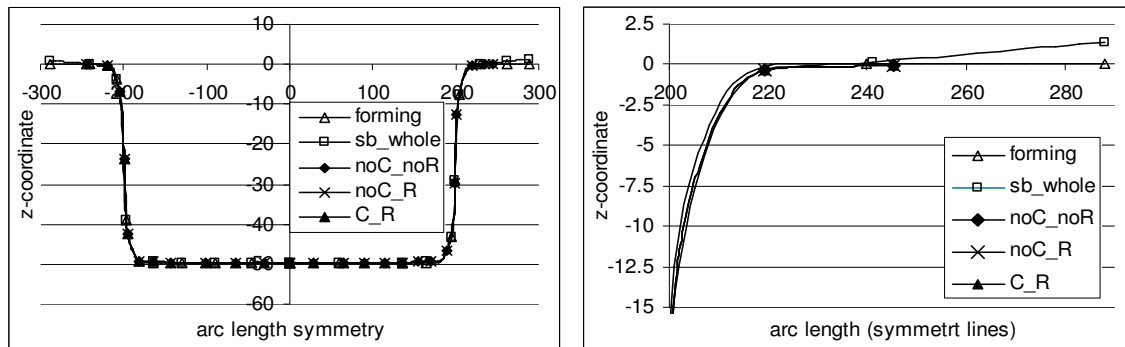
Figure 32 (c): Plate shape after forming along lines of symmetry (B-O-A) and (B*-O-A*) for circular cup (*Trimline 1*).

5.4   S-Rail

Next the attention is directed to the question if, for instance, the S-Rail, a less stiff product than a quarter of a rectangular (or a circular) cup studied before, shows a larger sensitivity in springback for the applied mapping algorithms. The S-Rail deep drawing problem was a benchmark problem at the Numisheet '96 conference [9]. This benchmark was designed to compare simulations and experiments for shape distortion, wrinkling and springback. In Figure 33 the simulation setup of the model for the springback analysis is shown.
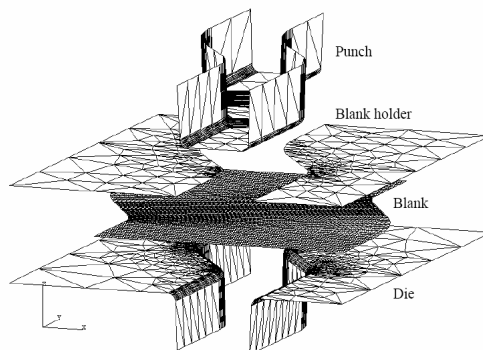
Figure 33: Simulation setup for S-Rail.

The dimensions of the blank are given in Figure 34. The dotted lines in this figure give the major dimensions of the punch and the die. The measures printed in *italics* at the bottom of the blank belong to the punch. The measures printed in *italics* at the top belong to the die, just as *italics* printed radii. The other punch and die radii are 5 mm.
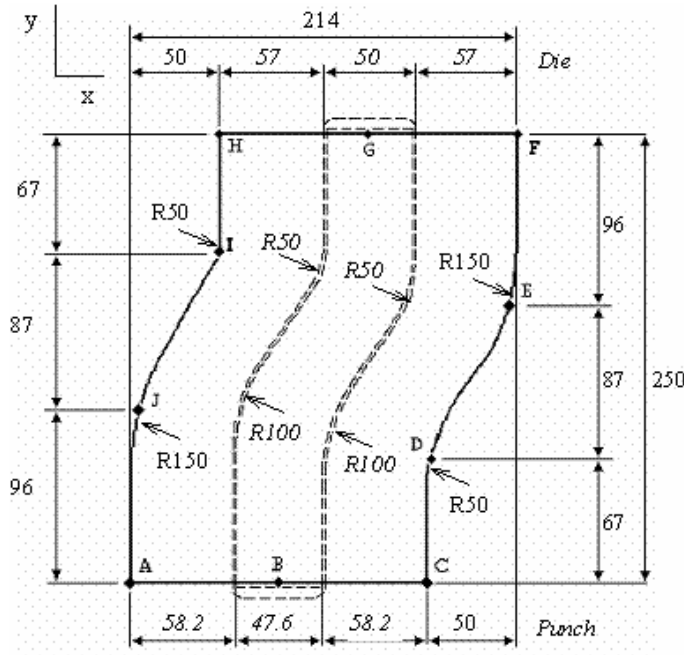

Figure 34: Schematic illustration of the S-Rail blank and the outline of the tools.

The S-Rail simulation is performed with DST3D elements with three integration points in-plane and five integration points in thickness direction. The blank is meshed with elements having a typical element size of 4 mm, which add up to total of 6000 elements. The product is positioned in *xy*-plane at $z = 0$. The rolling direction of the blank is taken along the y-axis. The blank material is a draw quality mild steel with a thickness of 1.0 mm. The material properties and the process parameters are listed in Table 4.

Material properties		Process parameters	
E	206000 N/mm^2	punch displacement	35 mm
v	0.3		
σ_{yield}	158 N/mm^2	blank holder force	100 kN
C	520 N/mm^2		
n	0.233	coefficient of friction	0.11
R_0, R_{45}, R_{90}	2.37, 1.52, 1.85		

Table 4 *Properties of the S-Rail problem*

This product is trimmed along several trimlines, see Figure 35. In present section, the numerical results obtained after trimming along *Trimline 1* will be appraised with respect to the effect of the influence of the mesh and data manipulation techniques on the amount

of springback. *Trimline 1* is a piece-wise linear line (A-B) that cuts off a band along the edge (flange) of a deep drawn S-Rail, i.e. the part of the blank clamped between the blank holder and the die during deep drawing. Two other trimlines are separating a part of the S-Rail by a single vertical plane, passing through two sets of trimline points; (C-D) for *Trimline 2* and (E-F) for the *Trimline 3*.The results for these two trimlines can be found in Appendix C.3.
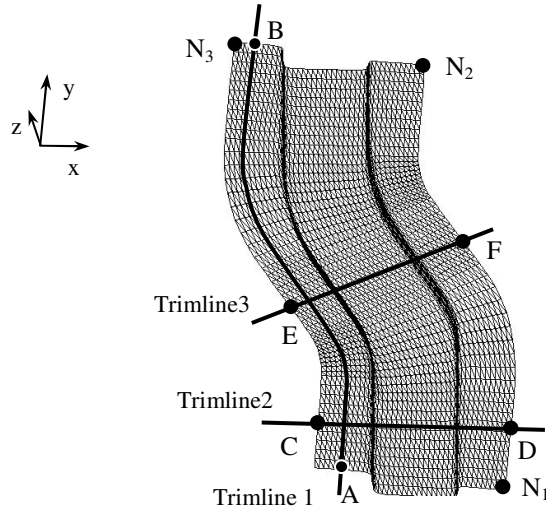

Figure 35: S-Rail with trimlines.

The springback deflection of this product due to its complexity is rather different from the deflection of the products already discussed. Some features of the sprung back shape of the S-Rail are the buckling tendency at the bottom of the product and twisting of the rail along the longitudinal direction. In order to suppress rigid body motions at the springback stage, specific degrees of freedom of three nodes N_1, N_2 and N_3 (see Figure 35) are fixed during the instantaneous springback.

S-Rail trimmed along the Trimline 1

The S-Rail, formed as was described previously, is trimmed along the *Trimline 1*, shown in Figure 35.
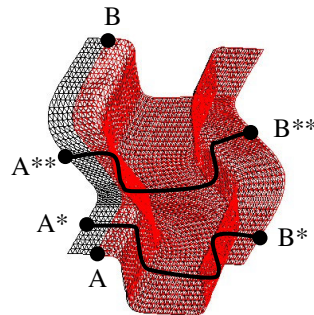
Figure 36 (a): S-Rail trimmed along the *Trimline 1*: formed (in black) and trimmed (in red); with plot levels (A*-B*) and (A**-B**).

During this trimming procedure, removing a part of the flange on one side of the product, the mesh reduced to 5478 elements. Results for this product are plotted along the vertical cross sections as shown in Figure 22 (d). Due to the complexity of the product the stress distribution after forming is different in various parts of the product. Therefore, plots along two different plot levels will be presented. Figures 36 (b) and (c) demonstrate the springback patterns of the S-Rail plotted along the transverse plot levels (A*-B*) and (A**-B**), respectively.

Figure 36 (b) shows results for the cross section (A*-B*) of the longitudinally straight part of the S-Rail.
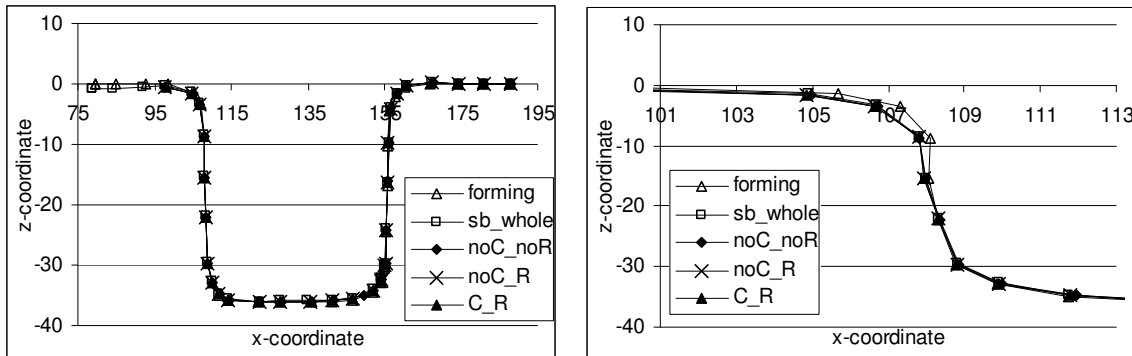
Figure 36 (b): Deflection of the S-Rail, trimmed by the *Trimline 1*, plotted along the level (A*-B*).

The bottom of the product in the left graph of the figure does not show buckling. All plotted patterns coincide at the bottom of the product. Three plots obtained after trimming with combinations of developed techniques are identical. Similar plots are shown for the cross section (A**-B**). Here, a very small bucking behavior is observed at the bottom of the product, which is detected in experiments as well. The springback pattern of the trimmed flange for all three patterns is identical and is about 0.3 mm larger than that for the untrimmed flange at $x = 69$ mm.
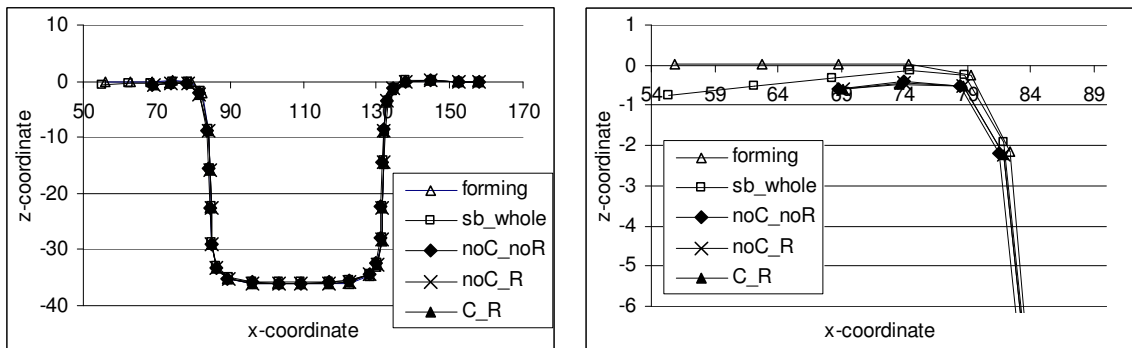
Figure 36 (c): Deflection of the S-Rail, trimmed by the *Trimline 1*, plotted along the level (A**-B**).

Similar results can be found in appendix for Trimline 2 and 3. Based on these results and the results discussed in Appendix C.3.1 and C.3.2, it can be concluded that the influence of the different remap algorithms on the springback behavior of the product stays within the plate thickness and therefore can be considered as negligible.

5.5   Scaled down car roof

Next, the scaled down car roof will be discussed. This product is chosen as the second component of the sensitivity analysis in the global Springback Project, because this product shows warping, an interesting non-symmetric springback phenomenon, which can be reproduced only by the full product modeling. However, for the purposes of studying the effects of trimming on the amount of springback only a quarter of the product is modeled. This product shows a buckling pattern in the sprung back flange shape, which sometimes gives raise to the problem of non-convergence of the springback calculation. The geometry of the tools and the blank are given in Figure 37. The product flange is positioned in *xy*-plane at $z = 0$. The punch stroke is -21 mm and the blank thickness is 0.595 mm.
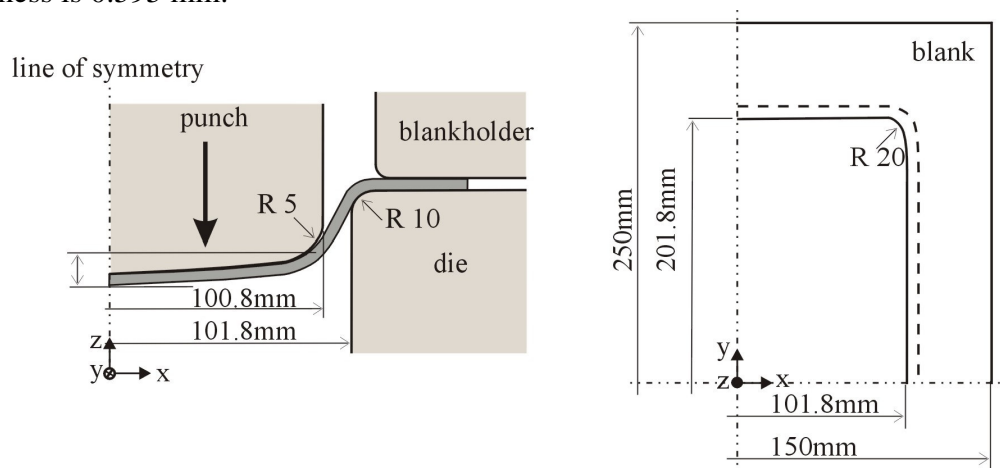
Figure 37: Tool geometry for scaled down car roof.

The bottom of the punch is doubly curved. The radius of curvature in length direction is 4000 mm, the radius of curvature in width direction is 1000 mm. The punch corner has a radius of 20 mm while the punch shoulder measures 5 mm. The die conforms the punch, taking into account an offset. The die shoulder radius is 10 mm.
The scaled down car roof is simulated with DST3D elements with three integration points in the plane and five integration points in the thickness direction. The edge of the blank is meshed with elements having a typical element size of 2.5 mm, while the inner part is meshed with elements with a typical element size of 7.5 mm, adding up to total of 8775 elements.

The blank material chosen is a high-strength low alloy steel (HSLA). The material properties and the process parameters are summarized in Table 5.

Material properties		Process parameters	
E	205000 N/mm^2	punch displacement	21 mm
ν	0.3		
σ_{yield}	277 N/mm^2	blank holder force	400 kN
C	645.5 N/mm^2		
n	0.18	coefficient of friction	0.14
R_0, R_{45}, R_{90}	0.981, 1.718, 1.54		

Table 5 *Properties of the Scaled down car roof simulated with HSLA*

In order to investigate the influence of the trimming accuracy improving techniques (with respect to springback) on this product, it was trimmed along a number of trimlines. In Figure 38 two representative trimlines cutting off a part of the quarter of a scaled down car roof are shown. The *Trimline 1* refers to the two-segment *box shaped* trimline (A*-B*-C*) and is described in present section. The second line is the straight trimline cutting of a part of the product flange (D-E). The results for the numerical trimming of the scaled down car roof along *Trimline 2* are comparable to the results obtained for the *Trimline 1*, see Appendix C.4.
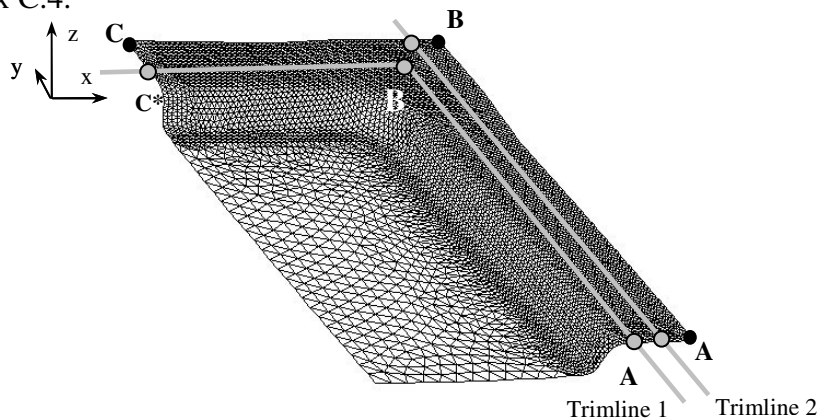
Figure 38: Quarter of the scaled down car roof with trimlines.

Scaled down car roof trimmed along the Trimline 1

In this section the performance of the developed algorithms within trimming will be tested on the quarter of a scaled down car roof trimmed along the *Trimline 1* (see Figure 38). During this trimming operation the mesh reduced to 5399 elements.
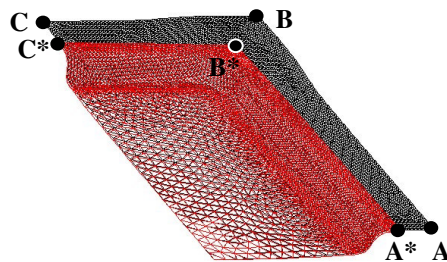
Figure 39 (a): Scaled down car roof trimmed along *Trimline 1*: formed (in black) and trimmed (in red).

In Figure 39 (b) the total amount of springback of the untrimmed flange measures up to 3.5 mm. After trimming this measure reduced to 2 mm for all flange patterns obtained after trimming. In fact, all three patterns coincide. As was already mentioned during the investigation of the effect of trimming, with various combinations of trimming improving techniques, on meshes with different element sizes, when mesh is fine the technique of in-plane data remapping does not have radical influence on the amount of springback. In Section 5.2.1 the mesh is referred to as fine if the size of the typical element in the trimming zone is about 3 mm. Thus, the result shown in Figure 39 (b) is consistent with the trend observed earlier and confirms the conclusions made in Section 5.2.1.
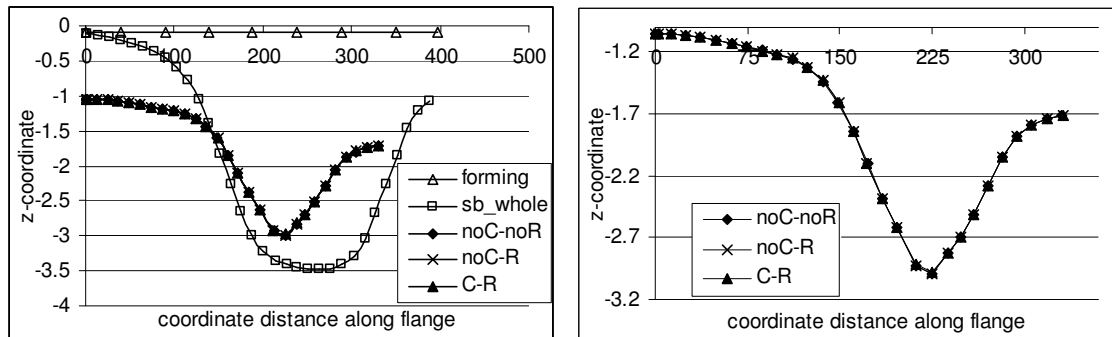
Figure 39 (b): Deflection of the flanges (A-B-C) and (A*-B*-C*) for scaled down car roof (*Trimline 1*).
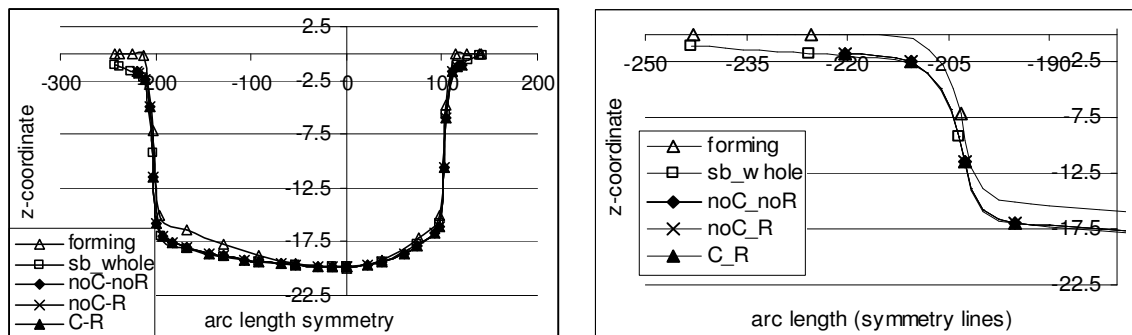
Figure 39 (c): Plate shape after forming along lines of symmetry (C-O-A) and (C*-O-A*) for scaled down car roof (*Trimline 1*).

The scaled down car roof was also simulated with a different material, namely the interstitial free steel (IF). The springback behavior observed in this case is different but the influence of the accurate data and mesh manipulation techniques in trimming is comparable to that detected for trimmed product simulated with HSLA steel. The results for trimming of the scaled down car roof simulated with the IF steel can be found in Appendix C.5.

5.6 Numerical results for 2D to the PLATE model transfer

This section shows the numerical results for the cutting stress transfer, as discussed in Chapter 4. The effect of the stress state transfer from 2D to the plate model is studied on the example of a quarter of a rectangular cup. The 2D cutting simulation was performed by a special purpose program, Crystal by Ruud Voncken (Philips BV). The geometrical framework for the simulations that were carried out in CRYSTAL was adopted from the thesis of Ruth van de Moesdijk [8]. The simulation setup is shown in Figure 40 and the geometric parameters are summarized in Table 6.
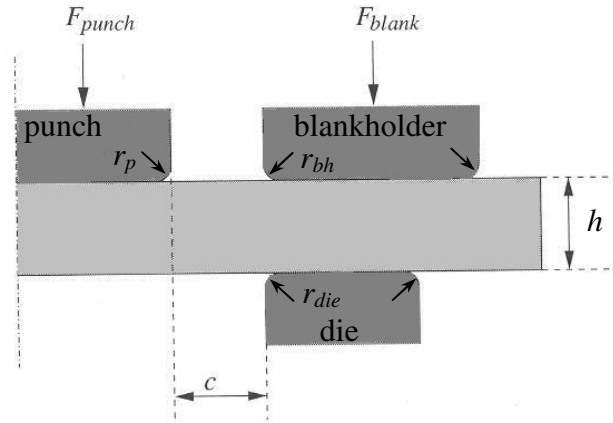
Figure 40: Schematic representation of the 2D cutting geometry setup.

r_{bh}	r_p	r_{die}	c
0.1 mm	0.1 mm	0.1 mm	15%

Table 6 *The geometric parameters*

In this simulation, a material with different properties is applied (compared to the material described in Section 5.2, Table 3). The plate model is built of discrete shear triangle elements with three integration points in the plane and five integration points in the thickness direction. The blank material properties and the process parameters for the deep drawing simulation are listed in Table 7. The blank thickness is 1 mm.

Material properties		Process parameters	
E	210000 N/mm^2	punch displacement	50 mm
v	0.3		
σ_{yield}	273 N/mm^2	blank holder force	50 kN
C	1228 N/mm^2		
n	0.40	coefficient of friction	0.14
R_0, R_{45}, R_{90}	1, 1, 1		

Table 7 *Properties and parameters of the rectangular cup deep drawing problem* (*material 2*)

Two sets of simulations are performed, one set makes use of the default mesh size (see Section 5.2.1) while the other set makes use of the fine mesh (see Section 5.2.1). Both sets are obtained by trimming of these meshes along the piecewise linear *Trimline 1* (see Figure 24). Each set consists of three simulations, i.e. a simulation without any of the discussed techniques, one simulation, which accounts for the centering and remap techniques only and one simulation which accounts for centering, remap and the cutting stress transfer. The focus of result discussing will be on the influence of the cutting stress transfer.

First the results for the default mesh will be discussed. Figures 41 and 42 show the zoom-in's of the z-coordinate of the flange and the x-axis of symmetry, respectively.
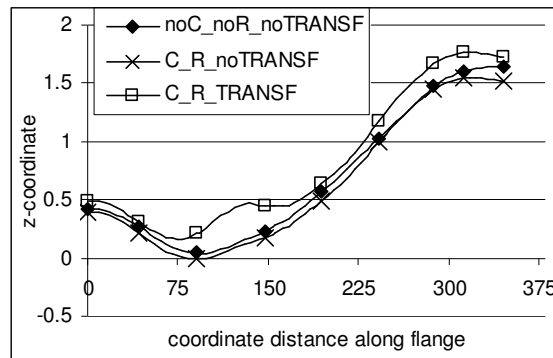
Figure 41: Deflection of the flange (A*-B*-C*) for default mesh (plate thickness 1 mm) with focus on cutting stress transfer

It can be seen clearly that the cutting stress transfer influences the springback pattern. The magnitude of this influence is around 25% of the plate thickness
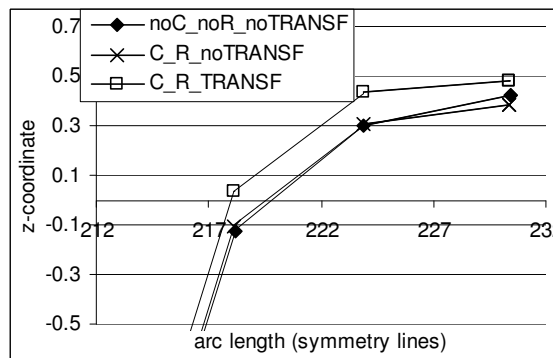
Figure 42: Zoom-in on the plate shape after forming along the x-axis of symmetry (O-A*) for default mesh (plate thickness 1 mm) with focus on cutting stress transfer

Second the results for the fine mesh will be discussed. Figure 43 and 44 show the z-coordinate of the flange and the x-axis of symmetry, respectively. In this set of simulations, it is even clearer that the cutting stress transfer influences the springback pattern; the magnitude is now around 40% of the plate thickness.

The difference between the influence of the cutting stress transfer on the magnitude of the springback for the different mesh sizes can be easily explained.
In the 2D simulation, high local stresses appear near the trimmed edge (note that the influence zone is only three times the plate thickness, see Chapter 4).
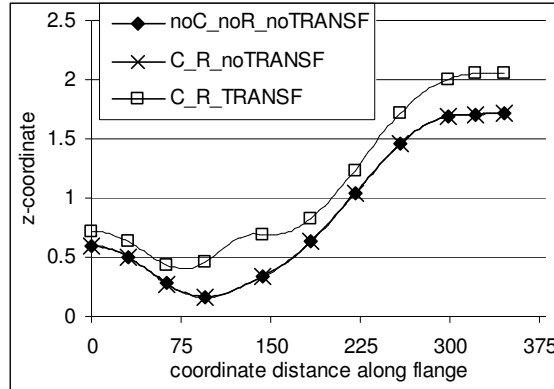

Figure 43: Deflection of the flange (A*-B*-C*) for fine mesh (plate thickness 1 mm) with focus on cutting stress transfer
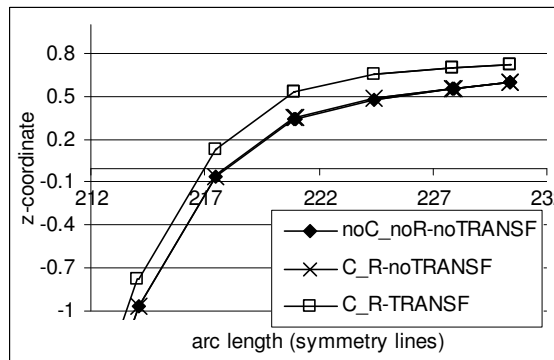

Figure 44: Zoom-in on the plate shape after forming along the x-axis of symmetry (O-A*) for fine mesh (plate thickness 1 mm) with focus on cutting stress transfer

In case of the fine mesh, the integration points of the plate element model, affected by the transfer algorithm, are much closer to the trimline, resulting in higher stress state compared to the default mesh, where the integration points are farther away from the trimline. Besides, the density of the integration points affected by the cutting stress transfer will be higher in case a fine mesh is used.

Conclusions

The transfer of the cutting stresses to the plate model results in a larger influence on the springback behavior than any combination of centering and remapping techniques. For meshes considered, the magnitude of the deflection after trimming with the transfer of the cutting stresses is around 40% of the plate thickness. This measure will be larger if a finer

57

plate model mesh will be employed in the zone affected by the cutting procedure, i.e. more plate model integration points will get data from the 2D model stress state.

Conclusions and recommendations

It can be concluded from the presented analysis that the influence of the centering and remapping techniques on the numerical springback is within 5-15 % of the plate thickness, whereas the imposition of transfer of the cutting stresses to the plate model results in shape change in springback of about 40 % of the plate thickness. The amount of the springback and the pattern of the flange deflection depend also on the choice of the product mesh and the trimline geometry.

- The finer the blank is meshed the bigger the amount of springback of the untrimmed flange.
- Remap makes sense if the new and the old meshes are distinctly different.
- When the mesh is fine the techniques such as mesh adaptivity and centering are not changing the shape of the elements to such extent that the data remap from the old to the new mesh will significantly influence the stress state.
- Quantitatively, the springback after trimming with superimposed remapping, centering and stress transferring techniques crops up to 5-40% of the plate thickness larger springback than after trimming without application of mentioned techniques. The total influence of all techniques, developed for more accurate description of the trimming operation with respect to the accuracy of springback prediction, stays within the plate thickness of the product. A springback change of this magnitude can be considered as negligible.

Recommendations:
- The trimming procedure can be extended to the trimming along the arc/circular line. The trimming will then be performed by 'circular blades', which will make the piece-wise linear approximation of the curved segments of the trimline unnecessary.
- The centering procedure can be improved by means of projection of the node with new averaged coordinates back on the tools. This will give the opportunity to trim the parts of the product that follow the tool radius/curvature.
- To make the 2D to 3D data transfer more accurate the elements along the trimline can be refined so that more integration point data will be processed.
- As a recommendation, another alternative of an accurate transfer of cutting stresses into the plate model can be developed, which comprises an Equivalent

Force-Moment model. This model has to account for a complete stress field in 2D, and then impose this Equivalent Force-Moment model on the trimmed edge.

Acknowledgements

Appendix A

Definition of the triangular coordinates

Given the global coordinates of the vertices of an arbitrary triangular element and of the point laying in this element the local triangular coordinates of this point can be defined.
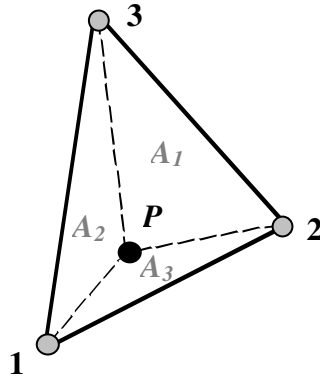

Figure A–1: Definition of the triangular coordinates

 The natural (local triangular) coordinate system for the triangular element is obtained by defining the three length ratios L_1, L_2 and L_3. Each coordinate is a length ratio that varies between zero and one. The coordinates L_1, L_2 and L_3 are also called *area coordinates* because their values give the ratio of the area of a subtriangular region, A_1, A_2 and A_3 respectively, to the area of the complete triangle.

$$L_i = \frac{A_i}{A}, \quad with \quad i = 1, 2, 3. \tag{A.1}$$

Since $A_1 + A_2 + A_3 = A$, an equation relating the three coordinates is:

$$L_1 + L_2 + L_3 = 1 \tag{A.2}$$

The area of the complete element *A* can be calculated in three stages. First, two vectors are constructed:

$$vec1 = \begin{Bmatrix} X_2 - X_1 \\ Y_2 - Y_1 \\ Z_2 - Z_1 \end{Bmatrix} \quad and \quad vec2 = \begin{Bmatrix} X_3 - X_1 \\ Y_3 - Y_1 \\ Z_3 - Z_1 \end{Bmatrix} \tag{A.3}$$

where *X*, *Y* and *Z*, with corresponding subscript, represent the coordinates of nodes 1, 2 and 3. Then the cross product of these two vectors is found.

$$vec3 = vec1 \times vec2 = \begin{bmatrix} \hat{i} & \hat{j} & \hat{k} \\ vec1(1) & vec1(2) & vec1(3) \\ vec2(1) & vec2(2) & vec2(3) \end{bmatrix} \qquad (A.4)$$

Finally, due to the fact that the value of the length of the vector $vec3$ equals the area of the parallelogram created by vectors $vec1$ and $vec2$, the area of the triangle is calculated as follows:

$$A = \frac{\sqrt{(vec3(1))^2 + (vec3(2))^2 + (vec3(3))^2}}{2} \qquad (A.5)$$

The area of the subtriangular region A_i is

$$A_i = \frac{1}{2}\begin{vmatrix} 1 & x & y \\ 1 & X_j & Y_j \\ 1 & X_k & Y_k \end{vmatrix}$$

where i, j and k are 1, 2 and 3 respectively and x and y are the coordinates if the point P. The remaining subtriangular regions are completed by cyclic permutation. The resulting expressions are:

$$A_1 = \frac{1}{2}\left[(X_2Y_3 - X_3Y_2) + (Y_2 - Y_3)x + (X_3 - X_2)y \right]$$

$$A_2 = \frac{1}{2}\left[(X_3Y_1 - X_1Y_3) + (Y_3 - Y_1)x + (X_1 - X_3)y \right] \qquad (A.6)$$

$$A_3 = \frac{1}{2}\left[(X_1Y_2 - X_2Y_1) + (Y_1 - Y_2)x + (X_2 - X_1)y \right]$$

The substitution of the expressions (A.6) in the equation (A.1) gives the triangular coordinates. The area coordinates (A.1) for the linear triangular element are identical to the shape functions, and the two sets or quantities can be interchanged.

Appendix B

Location of integration points through the plate thickness

The location of the integration points and their weight factor are summarized in the following table.

Number of integration points	Location	Weight factor
1	0.000000	2.
2	±0.577350	1.
3	±0.774597 0.000000	0.555556 0.888889
4	±0.861136 ±0.339981	0.347855 0.652145
5	±0.906176 ±0.538470 0.000000	0.236927 0.478629 0.568889
6	±0.932469 ±0.661209 ±0.238619	0.171324 0.360762 0.467914
7	±0.949107 ±0.741531 ±0.405845 0.000000	0.129485 0.279705 0.381830 0.417959
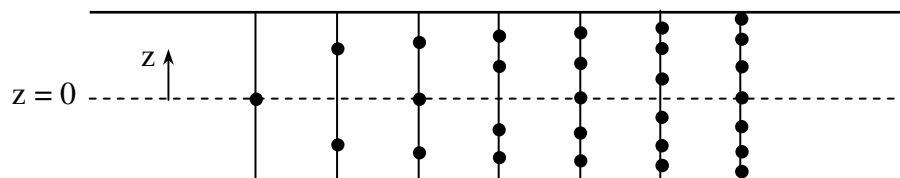
Figure B–1: Location of the integration points in thickness direction

Appendix C

Numerical results

The following examples are called to illustrate the effect of using the developed tools within trimming, such as centering (element shape improvement by means of node coordinate averaging) and remap, on the amount of springback of this product.

C.1 Rectangular cup trimmed along the Trimline 2

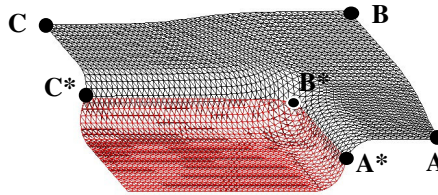The rectangular product meshed with the default mesh trimmed along the *Trimline 2* (see Figure 24). During trimming operation the mesh reduced from 4800 to 1941 elements.

Figure C.1 (a): Medium mesh trimmed along the *Trimline 2*: formed (in black) and trimmed (in red).
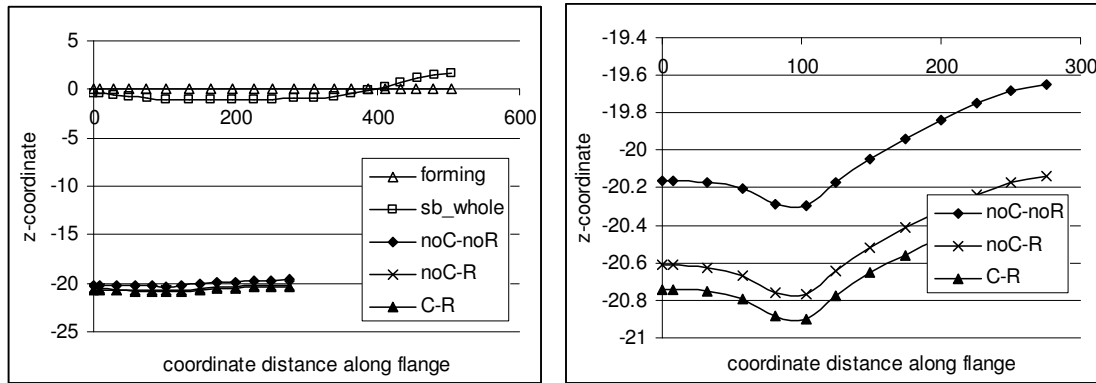
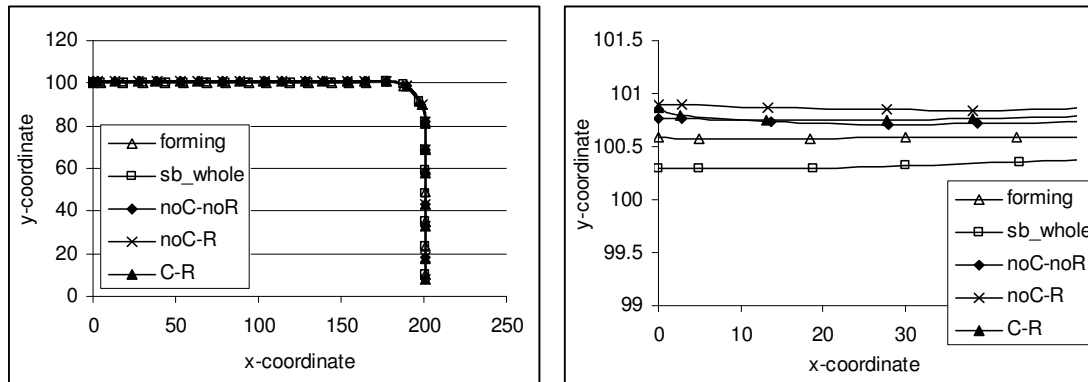**Figure C.1 (b):** Deflection of the flanges (A-B-C) and (D-E) for medium mesh.

Figure C.1 (c): Deflection of the wall of the product (E-D) at level *z* = -21 for medium mesh.
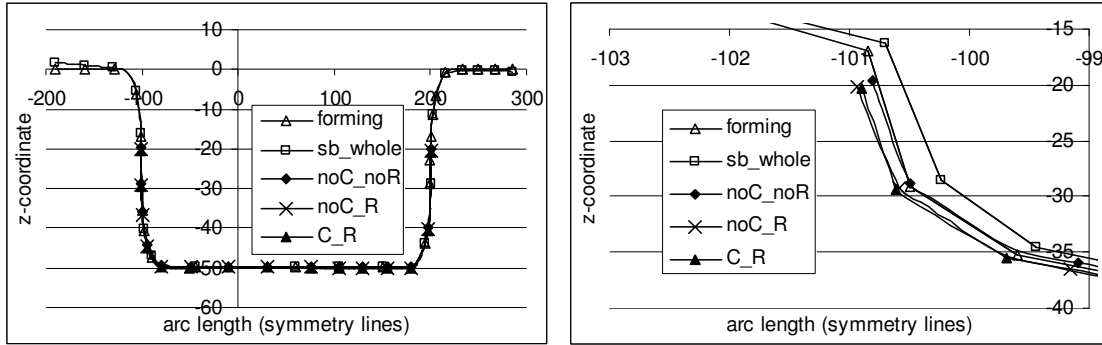
Figure C.1 (d): Plate shape after forming along lines of symmetry (C-O-A) and (E-O-D) for medium mesh.

C.2 Circular cup trimmed along the Trimline 2

The circular cup, as presented in Section 5.3, is trimmed along the *Trimline 2* (see Figure 31). During trimming operation the mesh reduced from 7079 to 3498 elements.
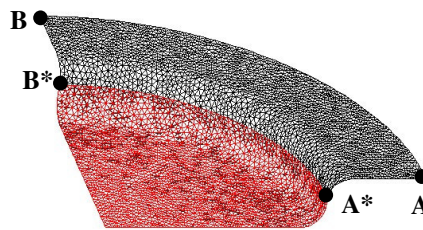

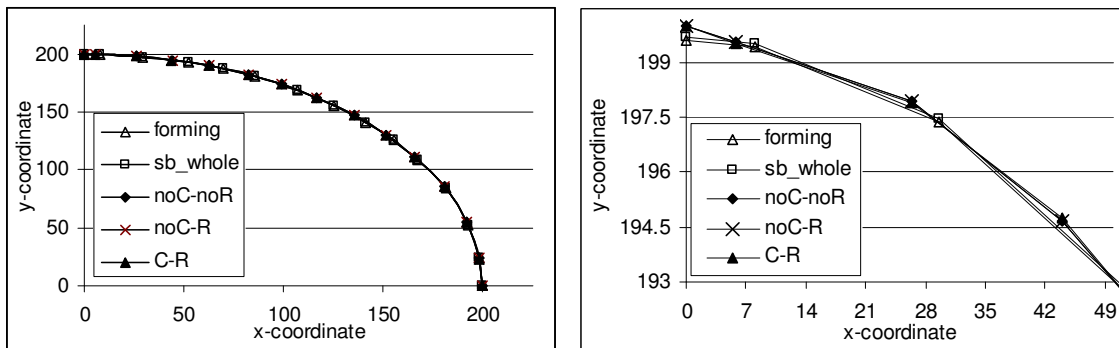**Figure C.2 (a):** Circular cup trimmed along the *Trimline 2*: formed (in black) and trimmed (in red).

Figure C.2 (b): Deflection of the flanges (A-B) and (A*-B*) for circular cup (*Trimline 2*).
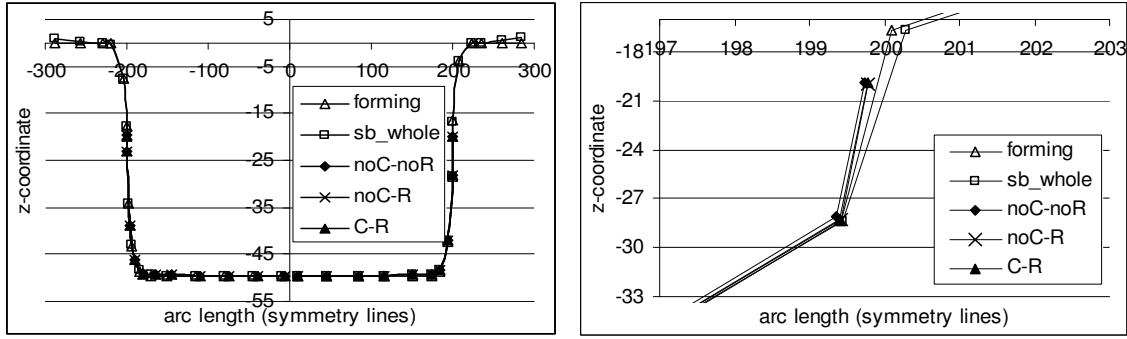
65

Figure C.2 (c): Plate shape after forming along lines of symmetry (B-O-A) and (B*-O-A*) for circular cup (*Trimline 2*).

C.3 S-Rail trimmed along the Trimlines 2 and 3

Subsections C.3.1 and C.3.2 will concentrate on the results concerning *Trimline 2* and *Trimline 3*, respectively. Both trimlines are separating a part of the S-Rail by a single vertical plane, passing through two sets of trimline points; (C-D) for *Trimline 2* and (E-F) for the *Trimline 3*, as shown in Figure 35.

Note: The centering technique cannot be applied to the meshes trimmed through the product (wall) curvatures due to the deficiency of the centering algorithm that averages all coordinates of the treated nodes, which as a result 'penetrate the tool'.

C.3.1 S-Rail trimmed along the Trimline2

During trimming operation the mesh reduced from 6000 to 4920 elements.
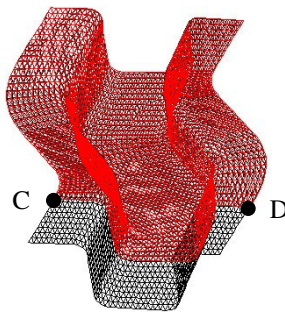

Figure C.3.1 (a): S-Rail trimmed along the *Trimline 2*: formed (in black) and trimmed (in red.
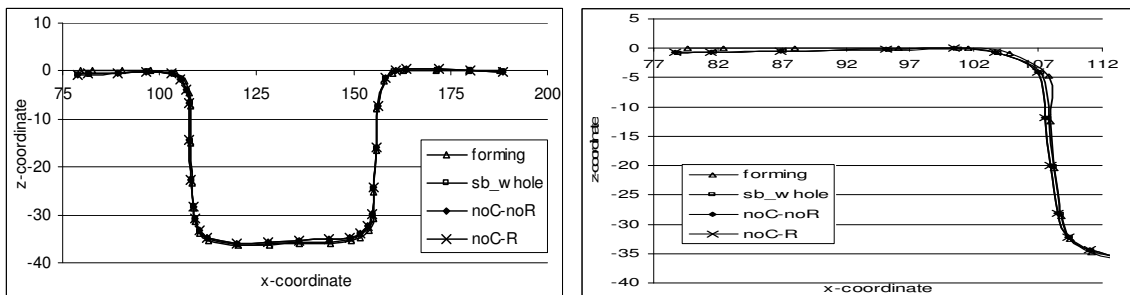

Figure C.3.1 (b): Deflection of the S-Rail, trimmed by the *Trimline 2*, plotted along the trimmed edge (C-D).

66

<u>C.3.2 S-Rail trimmed along the *Trimline 3*</u>
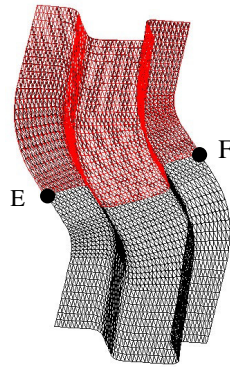During trimming operation the mesh reduced from 6000 to 2966 elements.

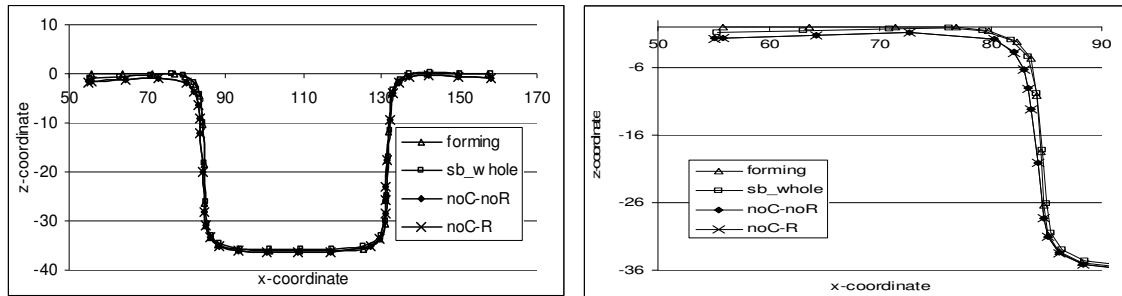**Figure C.3.2 (a):** S-Rail trimmed along the *Trimline 3*: formed (in black) and trimmed (in red.

Figure C.3.2 (b): Deflection of the S-Rail, trimmed by the *Trimline 3*, plotted along the trimmed edge (E-F).

C.4 Scaled down car roof trimmed along the Trimline 2
The next trimline considered is the straight trimline cutting off a part of the product by a single cutting plane (A*-B*), see Figure 38. The trimming in this case reduces the mesh to 6471 elements.
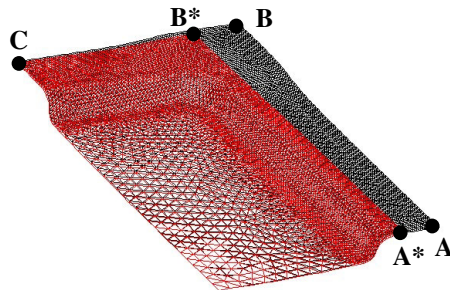

Figure C.4 (a): Scaled down car roof trimmed along *Trimline 2*: formed (in black) and trimmed (in red).
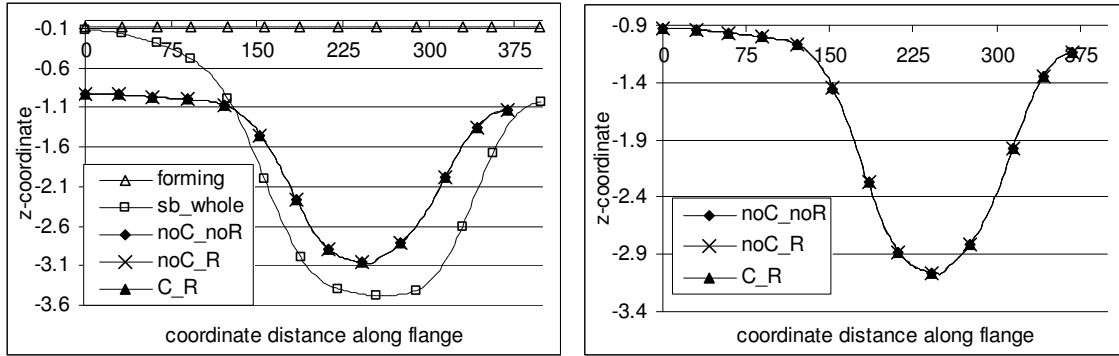
Figure C.4 (b): Deflection of the flanges (A-B-C) and (A*-B*-C) for car roof trimmed along *Trimline 2*.
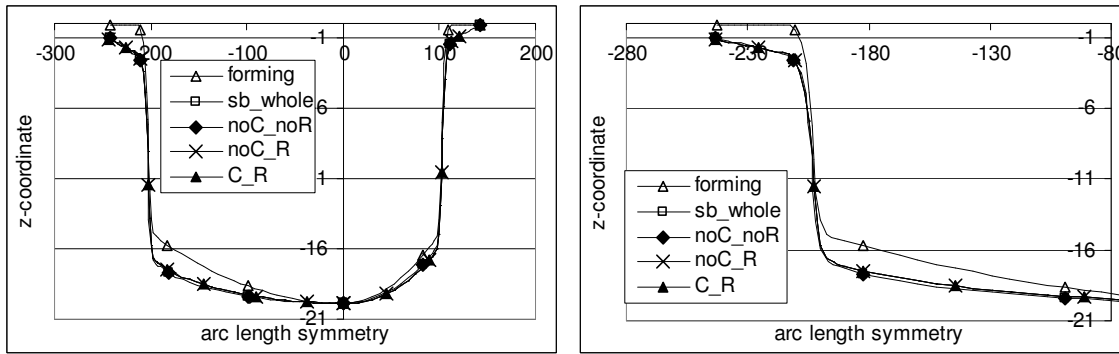

Figure C.4 (c): Plate shape after forming along lines of symmetry (C-O-A) and (C-O-A*) for car roof trimmed along *Trimline 2*.

C.5 Scaled down car roof simulated with Interstitial Free Steel

The developed trimming algorithm was also be applied to the scaled down car roof simulated with an interstitial free steel (IF). The geometry of the tools, the blank size and the meshing are similar to the setup of the simulation with HSLA steel (see Figure 37). The blank material properties and the process parameters for IF steel are listed in the following table.

Material properties		Process parameters	
E	205000 N/mm^2	punch displacement	20 mm
ν	0.3		
σ_{yield}	171 N/mm^2	blank holder force	400 kN
C	520 N/mm^2		
n	0.22	coefficient of friction	0.10
R_0, R_{45}, R_{90}	1.895, 1,592, 2.385		

Table C *Properties of the Scaled down car roof problem simulated with IF steel*

The product is trimmed along the *Trimline 1*, i.e. the *box shaped* line, see Figure 38. During this operation the mesh reduced from 8775 elements to 5571 elements.
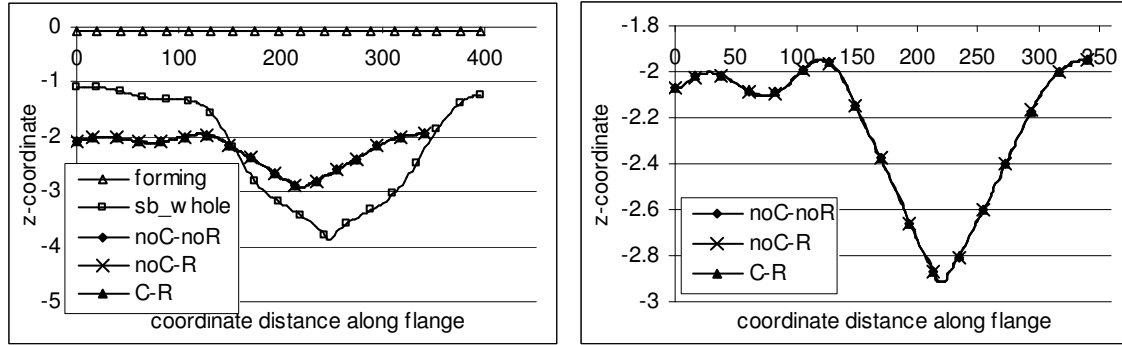
Figure C.5: Deflection of the flanges (A-B-C) and (A*-B*-C*) for scaled down car roof simulated with IF steel (*Trimline 1*).

The results obtained for springback after trimming with different techniques are similar to the ones described in Section 5.5 for the HSLA steel.

Each of the simulations of the springback of a car roof simulated with different materials runs for a specific set of parameters, such as blank holder force, damping, yield stress, friction, number of increments in springback step etc. The problems encountered concern the divergence of the solution in springback step. The results shown in Figure C.5 are obtained after instantaneous springback in 15 subincrements, whereas the results shown in Figure 39 (b) present the flange deflection of the product simulated with HSLA steel after numerical instantaneous springback performed in one (sub)increment.

For a consistent comparison of these simulations the gradual tool release has to be employed (for both), which imitates the reality when the punch and the blank holder are withdrawn (in real time frame) and the product is taken out of the die. This falls out of the scope of the present research goals.

List of Symbols

A	area
c	horizontal clearance
C	Nadaï parameter
d	distance, punch displacement
det	determinant
E	Young's modulus (modulus of elasticity)
F	force
h	thickness
$\hat{i}, \hat{j}, \hat{k}$	unit vector
IP	integration point
L	triangular coordinates;
	shape functions for triangular element
M	inverse of the Gauss interpolation matrix
n	n-value, hardening parameter
N	Gauss interpolation matrix
N_i	position coordinates of node i,
	shape functions for bulk element
N_{new}	position coordinates of new centered node
$N^{(4)}$	interpolation matrix for bulk element
$N^{(4)}_{inverse}$	inverse of the interpolation matrix for bulk element
$normal$	normal vector
P	point
Q	scaling parameter
r	tool shoulder radius
R	anisotropy parameter,
	radius
vec	vector
x, y, z	Cartesian coordinate axes
x_{IP}, y_{IP}	coordinates of integration point
x_P, y_P	coordinates of point P
X, Y, Z	coordinates of rotated triangular element
α, β, γ	unknown quantities in a set of algebraic equations
ε	strain
ε_{EQ}	equivalent plastic strain
ζ	state variable
η, ξ	natural coordinates
θ	angle
ν	Poisson's ratio

σ	normal stress (tensor)
σ_{yield}	yield stress
σ_{EQ}	equivalent stress
τ	shear stress

Coefficients

a, b, c, d

$a_1^*, a_2^*, a_3^*, a_4^*$

k_1, k_2, k_3

$x_1^*, x_2^*, x_3^*, x_4^*$

References

1. Avetisyan M., Meinders T., Huétink J., In: Proceed. ESAFORM 7, Trondheim (2004) 77-80.

2. Avetisyan M., Meinders T., Huétink J., *Influence of an Accurate Trimming operation on Springback*, International Journal of Forming Processes, to be published.

3. Boogaard A.H. van den, Thermally Enhanced Forming of Aluminum Sheet, Modeling and Experiments, PhD thesis, University of Twenty (2002).

4. Carleer B.D., *Finite Element Analysis of Deep Drawing*, PhD thesis, University of Twenty (1997).

5. Kawka M., T. Kakita and A. Makinouchi, *Simulation of Multi-Step Sheet Metal Forming Processes by a Static Explicit FEM Code*, Jour. Mat. Proc. Tech. 80 (1998) 54-59.

6. Lamers E.A.D., *Shape Distortions in Fabric Reinforced Composite Products due to Processing Induced Fiber Reorientation*, PhD thesis, University of Twente (2004).

7. Meinders V.T., *Developments in Numerical Simulations of the Real-life Deep Drawing process*, PhD thesis, University of Twente (2000).

8. Moesdijk R.D. van de, *Numerical Modeling of Shape Aberrations due to Blanking*, PhD thesis, University of Twente (1999).

9. Numisheet, 1996, *Proceedings of the 3rd International Conference on Numerical Simulations of 3-D Sheet Metal Forming Processes*, J.K. Lee et al. (eds.), Dearborn, Michigan, 1996.

10. Wagoner R.H., *Fundamental Aspects of Springback in Sheet Metal Forming*. In: Proceed. NUMISHEET'02, eds, D.-Y. Yang, S.I. Oh, H. Huh, Y.H. Kim, Jeju Island (2002) 13-24.

11. Wagoner R.H., W. Gan, K. Mao, S. Price, F. Rasouli, *Design of Sheet Forming Dies for Springback Compen-sation*. In: Proceed. ESAFORM 5, Salerno (2003) 7-14.

12.   Wenner A.L., *Work Hardening and Springback in Plane Strain Draw Forming*. In: Jour. Appl. Metalworking, 2 (2983) 277-285.

13.   Wisselink H.H., *Analysis of Guillotining and Slitting, Finite Element Simulations*, PhD thesis, University of Twente (2000).

14.   Zimniak Z., Tooling Design Compensating Springback Error after Deep Drawing and Trimming Operations. In: Proceed. ESAFORM 5, Krakow (2002) 531-534.